Comparison of NTF Experimental Data with CFD Predictions from the Third AIAA CFD Drag Prediction Workshop

John C. Vassberg[*], Edward N. Tinoco[*], Mori Mani[*]

The Boeing Company, Huntington Beach, CA 92647, Seattle, WA, 98124, St. Louis, MO, 63301, USA

David Levy[†], Tom Zickuhr[‡]

Cessna Aircraft Company, Wichita, KS 67218, USA

Dimitri J. Mavriplis[§]

University of Wyoming, Laramie, WY 82071, USA

Richard A. Wahls[¶], Joseph H. Morrison[‖]

NASA Langley Research Center, Hampton, VA 23681, USA

Olaf P. Brodersen[**], Bernhard Eisfeld[**]

DLR Institute of Aerodynamics and Flow Technology, 38108 Braunschweig, Germany

Mitsuhiro Murayama[**]

Japan Aerospace Exploration Agency (JAXA), Tokyo, 182-8522, Japan

Abstract

Recently acquired experimental data for the DLR-F6 wing-body transonic transport configuration from the National Transonic Facility (NTF) are compared with the database of computational fluid dynamics (CFD) predictions generated for the Third AIAA CFD Drag Prediction Workshop (DPW-III). The NTF data were collected after the DPW-III, which was conducted with *blind* test cases. These data include both absolute drag levels and increments associated with this wing-body geometry. The baseline DLR-F6 wing-body geometry is also augmented with a side-of-body fairing which eliminates the flow separation in this juncture region. A comparison between computed and experimentally observed sizes of the side-of-body flow-separation bubble is included. The CFD results for the drag polars and separation bubble sizes are computed on grids which represent current engineering best practices for drag predictions. In addition to these data, a more rigorous attempt to predict absolute drag at the design point is provided. Here, a series of three grid densities are utilized to establish an asymptotic trend of computed drag with respect to grid convergence. This trend is then extrapolated to estimate a grid-converged absolute drag level.

[*]Boeing Technical Fellow
[†]Senior Specialist Engineer
[‡]Principal Engineer
[§]Professor Mechanical Engineering
[¶]Project Scientist, Subsonic Fixed Wing / Fundamental Aeronautics Program
[‖]Assistant Head, Computational AeroSciences Branch
[**]Research Engineer

Nomenclature

AR	Wing Aspect Ratio $= \frac{b^2}{S_{ref}}$		N	Total Number of Grid Points
a	Acoustic Speed		NTF	National Transonic Facility
b	Wing Span		P	Static Pressure
BL	Butt Line Coordinate		q	Dynamic Pressure $= \frac{1}{2}\rho V^2$
CFD	Computational Fluid Dynamics		$RANS$	Reynolds-Averaged Navier-Stokes
C_D	3-D Drag Coefficient $= \frac{Drag}{q_\infty S_{ref}}$		Re	Reynolds number $= \frac{\rho_\infty V_\infty C_{ref}}{\mu_\infty}$
C_{DP}	Idealized Profile Drag $= C_D - \frac{C_L^2}{\pi AR}$		S_{ref}	Reference Area
C_{Dpr}	Pressure Drag Coefficient		SOB	Side-of-Body
C_{Dsf}	Skin-Friction Drag Coefficient		T	Temperature
C_L	Lift Coefficient $= \frac{Lift}{q_\infty S_{ref}}$		TE	Wing Trailing Edge
$C_{L\alpha}$	Lift Curve Slope		V	Velocity
C_M	Pitching Moment Coefficient		WB	Wing/Body
C_P	Pressure Coefficient $= \frac{P - P_\infty}{q_\infty}$		$WBNP$	Wing/Body/Nacelle/Pylon
C_{ref}	Wing Reference Chord $\simeq$ MAC		WT	Wind Tunnel
c_f	Local Coefficient of Skin Friction		Y^+	Wall Distance $= Re\sqrt{\frac{c_f}{2}}y$
$count$	Drag Coefficient Unit $= 0.0001$		α	Angle of Attack
DPW	Drag Prediction Workshop		Δ	Difference in Quantity
FS	Fuselage Station Coordinate		η	Fraction of Wing Semi-Span
LE	Wing Leading Edge		μ	Fluid Viscosity
MAC	Mean Aerodynamic Chord		ρ	Fluid Density
			∞	Signifies Freestream Conditions

I.   Introduction

The AIAA CFD Drag Prediction Workshop (DPW) Series was initiated by a working group of members from the AIAA Applied Aerodynamics Technical Committee. From the onset, the DPW organizing committee defined and has adhered to a set of primary objectives for the DPW Series. These include:

- Assess state-of-the-art computational fluid dynamics (CFD) methods as practical aerodynamic tools for the prediction of forces and moments on industry-relevant geometries, with a focus on absolute drag.

- Provide an impartial international forum for evaluating the effectiveness of CFD Navier-Stokes solvers.

- Promote balanced participation across academia, government labs, and industry.

- Use common public-domain subject geometries, simple enough to permit high-fidelity computations.

- Provide baseline grids to encourage participation and help reduce variability of CFD results.

- Openly discuss and identify areas needing additional research and development.

- Conduct rigorous statistical analyses of CFD results to establish confidence levels in predictions.

- Schedule open-forum sessions to further engage interaction among all interested parties.

- Maintain a public-domain accessible database of geometries, grids, and results.

- Document workshop findings; disseminate this information through publications and presentations.

The first workshop[1] in this series, DPW-I , was held in Anaheim, CA in conjunction with the 19th Applied Aerodynamics Conference of June 2001. The premise of DPW-I was to solicit CFD predictions of a common, industry relevant geometry and assess the results using statistical analysis techniques. Although the focus of the workshop was on drag prediction, lift and pitching moment predictions were also evaluated. The DLR-F4 wing-body configuration was chosen as the subject of DPW-I both because of its simplicity and the availability of publicly released experimental test data.[2] The workshop committee provided a standard set of multi-block structured, overset, and unstructured grids for the DLR-F4 geometry to encourage participation in the workshop and reduce variability in the CFD results. However, participants were also encouraged to construct their own grids using their *best practices* so that knowledge concerning grid generation and drag

prediction might be shared[3] among workshop attendees. The test cases were chosen to reflect the interests of industry and included a fixed-C_L single point solution, drag polar, and constant-C_L drag rise data sets. Eighteen participants submitted results, using 14 different CFD codes; many submitted multiple sets of data exercising different options in their codes, e.g., turbulence models and/or different grids. A summary of these results was documented by the DPW-I organizing committee.[4,5] Because of strong participation, DPW-I successfully amassed a CFD data set suitable for statistical analysis.[6,7] However, the results of that analysis were rather disappointing, showing a 270-drag-count spread in the fixed-C_L data, with a 100:1 confidence interval of more than ± 50 drag counts.

Despite the disheartening results of the statistical analysis, DPW-I was a definitive success. It brought together CFD developers and practitioners and focused their efforts on a common problem. It facilitated an exchange of best practices and promoted open discussions, identifying areas requiring further research or additional scrutiny. Possibly most significant, it employed statistical methods to objectively assess CFD results. Finally, it reminded the CFD and applied aerodynamics communities that CFD is not yet a fully matured discipline.

In addition to the accomplishments listed above, DPW-I initiated interest in industry-relevant drag predictions that has been sustained through two more workshops, and looks to continue beyond. Several of the participants presented their DPW-I results[8–12] at a well-attended special session of the 2002 AIAA Aerospace Sciences Meeting and Exhibit in Reno, NV. The interest generated by DPW-I naturally led to the planning and organization of the 2nd AIAA Drag Prediction Workshop, DPW-II. The DPW-II organizing committee, recognizing the success of DPW-I, maintained its objectives for DPW-II.

The second workshop[13] was held in Orlando, FL in conjunction with the 21st Applied Aerodynamics Conference of June 2003. For this workshop, the DLR-F6 was chosen as the subject geometry, in both wing-body (WB) and wing-body-nacelle-pylon (WBNP) form. The DPW-II organizing committee worked with DLR and ONERA to make pertinent experimental data available to the public domain. One specific objective of DPW-II was the prediction of the incremental drag associated with nacelle/pylon installation. Although the F6 geometry is similar to that of the F4, its pockets of flow separation at the design condition are more severe; these occur predominantly at the wing/body and wing/pylon juncture regions. Again, this workshop was documented with a summary paper,[14,15] a statistical analysis,[16] an invited reflections paper[17] on the workshop series, and numerous participant papers[18–30] in two special sessions of the 2004 AIAA Aerospace Sciences Meeting in Reno, NV. A conclusion of DPW-II was that the separated flow regions made it difficult to draw meaningful conclusions with respect to grid convergence and drag prediction. During the follow-up open-forum discussions, the CFD community voiced the desire for the organizing committee to include in the third workshop: a) *Blind Test Cases*, and b) *Simpler Geometries*. The request for blind test cases is motivated by an earnest attempt to better establish a measure of the CFD community's capability to predict absolute drag, rather than match it after-the-fact. The request for simpler geometries allows more extensive research in studies of asymptotic grid convergence.

The third workshop[31] was held in San Francisco, CA in conjunction with the 24th Applied Aerodynamics Conference of June 2006. The DLR-F6 WB from DPW-II was retained as a baseline configuration for the DPW-III to provide a bridge between these two workshops. However, to test the hypothesis that the grid-convergence issues of DPW-II were the direct result of the large pockets of flow separation, a new wing-body fairing was designed to eliminate the side-of-body separation. Details of the FX2B fairing design were documented by Vassberg *et al.*[32] In addition, to help reduce the wing upper-surface trailing-edge flow separation, a higher Reynolds number was introduced for the WB test cases. These changes in both geometry and flow condition also provided the DPW-III participants a blind test since no test data was available prior to the workshop. A total of 26 sets of CFD results for the DLR-F6 WB test cases were submitted by 15 participants from around the world. Results of the DPW-III are documented by papers presented at the 2007 AIAA Aerospace Sciences Meeting[33–38] and published in a Special Section of the AIAA Journal of Aircraft on the Drag Prediction Workshop.[39–44]

After DPW-III was completed, work was immediately underway at NASA and the DLR for a September 2007 test of a refurbished DLR-F6 model in NASA's National Transonic Facility (NTF). The goal of the test was to provide experimental data for comparison to existing DPW-III calculations with and without the Boeing-designed side-of-body fairing and at a Reynolds number higher than in the existing database. DLR provided all model hardware, including the new side-of-body fairing and mounting block to attach to the NASA balance. NASA provided instrumentation, new model support hardware (closely matching ONERA hardware used in earlier tests), and NTF test time. The maximum Reynolds number was 5 million based on mean aerodynamic chord, due to load limitations on the model and support hardware, and because the

existing model was not suitable for cryogenic conditions. To match existing data, the test matrix includes runs at a Reynolds number of 3 million at Mach numbers from 0.4 to 0.8. The clean-wing configuration with and without the new side-of-body fairing was included. Data acquired includes forces, moments, surface pressures, and wing deformations under load. Flow visualizations include transition measurements via sublimating chemicals, and techniques to visualize the side-of-body and wing trailing-edge flow separations. The results of this NTF wind-tunnel test are documented by Gatlin *et al.*[45] and included herein for comparison with the CFD database predictions of DPW-III. A companion paper which describes the aero-elastic wing deformations of the DLR-F6 wing-body as tested in the NTF is provided by Burner *et al.*[46]

When the concept of this workshop series first began to take form in January of 2000, it was impossible then to imagine the magnitude of the cumulative efforts the DPW participants would be willing to invest. Even in retrospect, this is hard to believe. It is a testament that a grass-roots campaign such as this workshop series can accomplish so much. Through the contributions of the DPW participants, the public now has access to a wealth of previously-unavailable CFD data.

This paper is organized in the following manner. Section II provides a description of the subject configurations. Section III outlines the test cases of the third workshop. Section IV gives a brief description of the family of baseline grids utilized in the workshop. Section V compares the NTF experimental data with the collective results of the DPW-III. Section VI outlines our on-going plans in preparation for DPW-IV. Tables of data are embedded within the text closely after first reference, while all figures are appended to the end of this publication.

II.   DLR-F6 Wing/Body and FX2B Fairing Geometries

The baseline WB configuration for DPW-III was the DLR-F6 wing/body which was the same geometry used as the test case in DPW-II. The F6 wind tunnel model represents an aircraft designed to cruise at transonic speeds with a wing leading-edge sweep of $27.1°$ and a quarter-chord sweep of $25°$. The dihedral of the wing is $4.787°$. More reference quantities for this model are provided below.

$S_{ref}/2$	$72,700.0\ mm^2$		X_{ref}	$157.9\ mm$
C_{ref}	$141.2\ mm$		Y_{ref}	$0.0\ mm$
$b/2$	$585.647\ mm$		Z_{ref}	$-33.92\ mm$

Note that an aspect ratio of 9.5 is used herein instead of the computed value of 9.436. The purpose of this is to remain consistent with the literature on this geometry. A planform view of the F6 WB configuration is shown in Figure 1. For more detailed information on this geometry, see Brodersen *et al.*[47] and Laflin *et al.*[14]

The DLR-F6 model has an acute angle, roughly $60°$, between the fuselage and wing upper-surface at the trailing-edge which contributes or leads to flow separation at the WB juncture. A new WB fairing was developed by Vassberg *et al.*[32] with the goal of completely removing the separation bubble present at the design conditions. For consideration of a possible follow-on wind-tunnel test, the only design constraint for this fairing was that it does not cut into the baseline DLR-F6 geometry. Further, no attempt was made to optimize drag reduction. By removing the side-of-body pocket of flow separation, this workshop could test the hypothesis that the complexity associated with flow separations is the root cause of the poor asymptotic grid convergence identified in DPW-II.

III.   Test Cases

The success of the DPW Series is due in large part to the significant amount of personal time and computing resources invested by the participants of the workshops. In order to keep these individual investments from growing out of control, the organizing committee decided to essentially manage DPW-III as two sub-workshops within one. This document focuses on presenting data from the first test case; for reference, we also describe the second test case. Participants were allowed to select one of the following two cases, but were then required to provide all data mandated for that test case. Both cases are blind tests, the first on rather simple wing/body configurations, the second on extremely simple wing-alone shapes. Both cases include a single-point grid-sensitivity study, and an alpha-sweep on a medium-size grid. Note that a fixed-lift

condition requires convergence on α; this in turn adds additional effort. In addition, the CFD solutions for both test cases were required to represent fully turbulent flow as closely as possible.

In order to collect a consistent set of data from each participant, the organizing committee supplied template dataset files. These templates requested lift, drag (broken down by mechanical component), pitching moment, pressure distributions at specified span stations, trailing-edge separation locations, dimensions of the side-of-body separation bubble, grid family and sizes, turbulence model, computing platform and code performance, number of processors used, number of iterations required, etc. These workshops capture an extensive amount of information that serves as a snapshot of the industry capabilities of the time. For example, in the three workshops held thus far, one obvious trend is that the size of a typical wing/body grid has grown dramatically; the average size of the Medium WB structured-meshes in DPW-I, DPW-II and DPW-III have been 3.2, 5.4 and 7.8 million grid points, respectively. This represents a growth rate of 30% per year between DPW-I and DPW-II, and 13% per year between the last two workshops. Does this indicate that engineering applications are finally approaching the grid resolutions needed for accurate drag predictions on a wing/body configuration? We will at least show that the engineering-class grid resolutions (DPW Medium grids) are likely within the asymptotic range of grid convergence for many, yet not all, of the solvers represented herein. However, even this assertion is the subject of on-going discussions.

Case 1: DLR-F6 WB with and without FX2B Fairing

The first test case is based on the DLR-F6 wing/body configuration. This case study was constructed to serve two purposes: *a*) provide a link to DPW-II, and *b*) test a hypothesis that pockets of flow separation can be a root cause for results showing poor grid convergence.

Participants were required to provide data for both the baseline DLR-F6 geometry and one that incorporates the FX2B fairing at the following flow conditions on the specified grids.

Fixed-C_L Single Point Grid Sensitivity Study on Three Grids

- $Mach = 0.75$, $C_L = 0.5$, $Re = 5$ million.

Drag Polar on Medium Grid

- $Mach = 0.75$, $Re = 5$ million, $\alpha = [-3.0°, -2.0°, -1.0°, -0.5°, 0.0°, 0.5°, 1.0°, 1.5°]$.

Case 2: DPW-W1/W2 Wing-Alone

The second test case is based on generic wing-alone geometries designed by members of the organizing committee. Participants were required to provide data for both wings at the following flow conditions on the specified grids.

Fixed-α Single Point Grid Sensitivity Study on Four Grids

- $Mach = 0.76$, $\alpha = 0.5°$, $Re = 5$ million.

Drag Polar on Medium Grid

- $Mach = 0.76$, $Re = 5$ million, $\alpha = [-1.0°, 0.0°, 0.5°, 1.0°, 1.5°, 2.0°, 2.5°, 3.0°]$.

As mentioned above, no further analysis of Case 2 is included in this paper.

IV.   Baseline Grids

An overview of the baseline grids is provided in this section. However, the details of these grids are not included herein. For more information regarding these grids, please refer to our companion papers on this topic. Tinoco *et al.*[34] provides descriptions of the Tinoco multiblock structured and AFLR unstructured grid families. Sclafani *et al.*[36] provides descriptions of the Sclafani overset structured grid families. Mavriplis[35] provides descriptions of the LaRC unstructured mesh families. Brodersen *et al.*[37] provides descriptions of the DLR hybrid mesh families.

Because of the variation of grid types needed, a set of gridding guidelines, listed below, was established to help facilitate the creation of these grids. The gridding guidelines were provided to the persons responsible for generating the baseline grids in an attempt to maintain some level of uniformity across all types of meshes. Note that each grid family is required to include a Coarse (C), Medium (M), and Fine (F) grid. Further, the organizing committee decided that the Medium mesh should be representative of current engineering applications of CFD being used to estimate absolute drag levels on similar configurations. For unstructured meshes, the size of the Medium mesh is also a function of the intended flow solver. For example, a cell-centered scheme has about 5.5 times the numbers of unknowns as that of a nodal scheme for a given unstructured tetrahedral mesh, with the ratio being closer to 3.5 for typical hybrid meshes. In the tables that follow, only number of grid points are given.

Table I provides the number of grid points for each grid family, configuration, and resolution for Case 1. The Tinoco through AFLR families were baseline grids provided by the organizing committee and are available to the public domain. (Although not shown in this table, the Tinoco grid family also includes a Medium-Fine mesh for both wing/body configurations.) The Embraer through TAS grids were generated by individual participants; they were not generally available before the workshop (they currently are) and are included here to document grid sizes to the extent known. The types of meshes used include multiblock (MB), overset (OS), unstructured (UN), and hybrid (HY); the LaRC grid family was used in unstructured and hybrid states (UH). These grids range in size from 2.3 to 41.1 million points. Also included in this table is a mapping of the participants who used each grid. The usage key is described in Section V.

Gridding Guidelines

- Boundary Layer Region

    - $Y^+ \leq [1, \frac{2}{3}, \frac{4}{9}]$ $[C, M, F]$
    - $\Delta_1 \sim 0.0006\ mm$, [Approximate dimensional spacing for $Y^+ = 1$]
    - $\Delta_2 = \Delta_1$, [Two cell layers of constant spacing at viscous wall]
    - Growth Rates ≤ 1.25, [Preferably ≤ 1.20]

- Farfield: $\sim 100\ C_{ref}$-lengths away from geometry

- Local Spacings on Medium Grid

    - Chordwise: 0.1% local chord at Wing Leading Edge & Trailing Edge
    - Spanwise: 0.1% semispan at root & tip
    - Cell Size on Fuselage Nose & Tail: 2% C_{ref}

- Cells across Wing Trailing-Edge Base: $[8, 12, 16]$ $[C, M, F]$

- Grid Family

    - Medium Mesh Representative of Current Engineering Drag Predictions
    - Maintain a Parametric Family of Uniformly-Refined Grids in Sequence
    - Grid Size to Grow $\sim 3X$ for Each Level Refinement [Structured: 1.5X in Each I,J,K Direction]
    - Give Consideration to Multigridable Dimensions on Structured Meshes
    - Sample Size for DLR-F6 Wing/Body: $[2.7M, 8M, 24M]$ $[C, M, F]$

V.   Results

Participants of the DPW-III were required to provide results on either the wing/body or wing-alone test case. To their credit, many participants chose to investigate both cases; several provided multiple datasets on a given case. This section summarizes the data collected on the wing-body test case. These data are then used to estimate absolute drag levels for the DLR-F6 with and without the FX2B fairing. These estimates are made prior to any experimental data being available (at test-case Reynolds number) on any

of the configurations. In total, there were twenty-six submissions for Case 1; these submissions are tagged with a single capitalized letter from A-Z.

A representative example of the wing pressure distributions at the design condition of $M = 0.75$, $C_L = 0.5$, and $Re = 5$ million is given in Figure 2. In this example, the 15% semispan (near side-of-body) upper-surface pressure distribution of the baseline DLR-F6 exhibits signs of flow separation, while the flow about the FX2B geometry shows no signs of separation. This side-of-body separation can be seen in both the NTF experimental data and the CFD results. However, the CFD solution of this figure has captured a much larger bubble than that exhibited in the NTF experimental test. In general, the DPW-III submissions unanimously agreed that the flow was attached for the FX2B configuration, however, they were divided dramatically on the size of the side-of-body separation bubble for the baseline DLR-F6. More discussion on this will follow.

Table I: Case 1 DLR-F6/FX2B Grids - Number of Grid Points.

Family	Type	DLR-F6			FX2B			Usage
		Fine	Medium	Coarse	Fine	Medium	Coarse	
Tinoco	MB	27,185,664	8,080,896	2,298,880	27,185,664	8,080,896	2,298,880	A-C,G-J
SAUNA	MB	9,761,201	4,731,073	2,551,989	9,761,201	4,731,073	2,551,989	D
Extruded	MB	28,367,120	9,343,009	2,996,626	28,367,120	9,329,185	3,028,420	E
Gridgen	MB	27,982,776	8,927,196	2,739,621	27,982,776	9,138,772	2,842,878	F,T
Sclafani	OS	26,892,352	7,985,236	2,387,918	26,969,192	8,020,348	2,395,170	K-M,U
DLR	HY	8,535,263	5,102,446	2,464,385	10,305,876	6,111,664	2,873,102	N
ANSYS	HY	18,120,772	8,038,922	3,059,189	20,472,520	8,272,308	3,163,605	O
LaRC	UH	40,014,934	14,298,135	5,354,214	41,069,036	14,598,610	5,618,073	P,Q
AFLR	UN	11,374,451	3,792,485	1,492,082	11,849,212	3,178,559	1,640,590	R,S,Y
Embraer	UN	24,030,000	8,320,000	3,550,000	24,030,000	8,320,000	3,550,000	V
STAR	UN	-	12,377,058	-	21,509,137	12,469,599	8,421,799	W
USM3D	UN	-	-	-	-	-	-	X
TAS	UN	17,535,215	9,431,154	5,399,929	17,219,535	9,481,477	5,422,128	Z

NTF Experimental Data Analysis

Experimental data from the NTF wind-tunnel test are provided by Gatlin et al.[45] The drag polars from Runs 106 & 96 of these data are shown in Figures 3-4, which correspond to the baseline DLR-F6 WB and the FX2B configuration, respectively. For the purpose of detail visual examination, these polars have been plotted as idealized drag instead of absolute drag. The published scatter on these data are $\Delta C_D = \pm 0.00014$ for the baseline DLR-F6 WB and $\Delta C_D = \pm 0.00019$ for the FX2B configuration.

In addition to the experimental data, least-squares curve fits of the idealized drag polars are also provided. A couple of observations will be made about the experimental data. The curve fits help illustrate that the data is very well behaved for $C_L \leq 0.15$, is slightly higher drag than the fits for $0.15 \leq C_L \leq 0.25$, has a singular low drag value for $C_L \approx 0.30$, and becomes a little more scattered for $C_L \geq 0.40$. Note that these subtle trends within the data are imperceptable if plotted as conventional drag polars, even though they exist. Since we are most interested at the drag levels at the design point of the DLR-F6, $M = 0.75$, $C_L = 0.5$, and $Re = 5$ million, we fit the NTF polars with data for $C_L \leq 0.53$. This gives the following equations related to the curves shown in Figures 3-4.

$$C_{DP.F6} = 0.013093\, C_L^2 - 0.005158\, C_L + 0.018454$$

$$C_{DP.FX2B} = 0.012477\, C_L^2 - 0.004676\, C_L + 0.018124$$

(1)

where

$$C_{DP} \equiv C_D - \frac{C_L^2}{\pi AR} = C_D - 0.033506\, C_L^2.$$

(2)

Eqn (2) with Eqns (1) also provide the least-squares fit of absolute drag. At the design point, the idealized profile and absolute drag levels per the fits are as follows.

$$
\begin{aligned}
C_{DP.F6} &= 0.01915 \pm 0.00014 \\
C_{DP.FX2B} &= 0.01891 \pm 0.00019 \\
\\
C_{D.F6} &= 0.02752 \pm 0.00014 \\
C_{D.FX2B} &= 0.02728 \pm 0.00019
\end{aligned}
\tag{3}
$$

The incremental effect of the FX2B fairing from the NTF data is then $\Delta C_D = -0.00024 \pm 0.00033$. Hence, the FX2B fairing could introduce a 1.1 count drag penalty at one extreme, or provide a 5.7 count improvement at the other.

Case 1: DLR-F6 WB with and without FX2B Fairing

Table II provides the CFD code, grid type, grid family, turbulence model, and submitter name and organization for each block of data submitted. Twenty of the twenty-six submissions were complete in the sense that they included all of the mandatory data requested. While almost all of the data were supplied by the six remaining, these data blocks could not be used to conduct a consistent Richardson extrapolation to the continuum in the grid-sensitivity study.

Table II: Case 1 Submissions.

Tag	Code	Grid Type	Grid Family	Turbulence Model	Submitter
A	PAB3D	Multiblock	Tinoco	Girimaji EASM	ASM Elmiligui
B	PAB3D	Multiblock	Tinoco	K-Epsilon	ASM Elmiligui
C	PAB3D	Multiblock	Tinoco	SZL EASM	ASM Elmiligui
D	STAR-CCM+	Multiblock	SAUNA	Wilcox K-Omega	QinetiQ Milne
E	UPACS	Multiblock	Extruded	Modified SA	JAXA Murayama
F	UPACS	Multiblock	Gridgen	Modified SA	JAXA Murayama
G	CFL3D-Thin	Multiblock	Tinoco	SA	Boeing Tinoco
H	CFL3D-Thin	Multiblock	Tinoco	SST	Boeing Tinoco
I	CFL3D-Full	Multiblock	Tinoco	SA	Boeing Tinoco
J	CFL3D-Full	Multiblock	Tinoco	SST	Boeing Tinoco
K	CFL3D-Full	Overset	Sclafani	SST	LaRC Rumsey
L	CFL3D-Thin	Overset	Sclafani	SST	LaRC Rumsey
M	Overflow	Overset	Sclafani	SA	Boeing Sclafani
N	TAU	Hybrid	DLR	SA Edwards	DLR Brodersen
O	Edge	Hybrid	ANSYS CFX	Hellsten EARSM	FOI Eliason
P	FUN3D	Unstructured	LaRC Nodal	SA	LaRC Lee-Rausch
Q	NSU3D	Hybrid	LaRC Mixed	SA	UWy Mavriplis
R	CFD++	Hybrid	AFLR	SA	Boeing Venkat
S	BCFD	Hybrid	AFLR	SA	Boeing Winkler
T	UPACS	Multiblock	Gridgen	SST	JAXA Murayama
U	OVERFLOW	Overset	Sclafani	SST	LaRC Rumsey
V	FLUENT	Unstructured	Embraer	K-Epsilon	Fluent Scheidigger
W	STAR-CCM+	Unstructured	STAR	SST	CD-Adapco Vaughn
X	USM3D	Unstructured	USM3D	SA/WF	Raytheon Venkat
Y	BCFD	Hybrid	AFLR	SST	Boeing Winkler
Z	TAS	Unstructured	TAS	Modified SA	JAXA Murayama

Case 1a: Fixed-C_L Single-Point Grid Sensitivity Study

Figures 5-8 provide grid-sensitivity trends for idealized profile drag at the single-point fixed-C_L condition. The blue horizontal lines in these figures depict the scatter band of the NTF data centered about the curve fits of Equations 1. In these figures, side-by-side comparison plots are shown, where the baseline DLR-F6 data is captured in the left plot and the FX2B data on the right. The curves of these plots are labeled with the tag letter given in Table II. Note that all data blocks based on the Tinoco grid family also include results from a Medium-Fine grid; for consistency, these data are not included in the tables, nor were they utilized in the ranking procedure described at the end of this subsection. Figure 5 includes all data from all submissions. At first glance of this overview plot, the scatter in this data can be quite disheartening. Recall that the Medium mesh is supposed to represent the current engineering practice. In these figures, the Medium mesh grid factor falls within the range [2E-05 , 3E-05]. Hence, the range of the idealized profile drag scatter of the current engineering practice is on the order of 50 counts, for either configuration. A paper by Morrison and Hemsch[33] addresses this scatter and better quantifies confidence levels through a rigorous statistical analysis of the data.

The composite curves of Figure 5 are broken out by grid type in Figures 6-8 and compared with the NTF data. Figure 6 illustrates the trend of the multiblock CFD results. In this figure, note that three different multiblock families are shown. The solid lines represent results using the Tinoco grid family; the dashed lines capture the Gridgen families; the chain-dot refer to the SAUNA grid family. For the DLR-F6 baseline, note that if extrapolated to the continuum, many of the Tinoco-grid-family results indicate a low-drag value, while the Gridgen-grid-family data point to a higher value. For the FX2B geometry, the data associated with these two grid families are more comparable. Figure 7 shows the grid-sensitivity trends for the Sclafani-grid-family of overset-grid results. Figure 8 provides the corresponding trends of the unstructured and hybrid CFD solutions. In this figure, note that the unstructured-mesh families are grouped. The solid lines represent results based on the LaRC grid families; the dashed lines depict results using the AFLR grid families; the chain-dot lines capture data based on the five remaining unstructured-mesh families.

If a Richardson extrapolation is performed on a pair of data from a grid-sensitivity curve, an estimate of the continuum value is obtained. If this extrapolation is performed using data from the Fine and Medium meshes, the resulting value does not necessarily equal that of a similar extrapolation using data from the Medium and Coarse meshes. If the two values are equal, the trend line is exactly straight, and thus meets the necessary (but insufficient) requirement that data from all three meshes fall within an asymptotic range. (Other requirements include: having a consistent family of grids, having sufficiently-converged solutions, having the correct order of the scheme, etc.) In the following Lagrange equation, let $\mathcal{Y}$ represent any one of the quantities α, C_D, C_{Dpr}, C_{Dsf}, or C_M , and $\mathcal{X} = N^{-\frac{2}{3}}$. Here, N is the total number of grid points in the grid system. As defined, $\mathcal{X}$ is an appropriate parameter for a second-order scheme applied to results on a parametric family of three-dimensional meshes that have been uniformly refined in all three coordinate directions.

$$\mathcal{Y}_{FM} = \frac{\mathcal{X}_M \mathcal{Y}_F - \mathcal{X}_F \mathcal{Y}_M}{\mathcal{X}_M - \mathcal{X}_F}. \tag{4}$$

Here, $\mathcal{Y}_{FM}$ represents the continuum estimate using the Fine/Medium pairs of data.

As mentioned earlier, only twenty of the submissions provided sufficient data to perform a consistent set of Richardson extrapolations. These data are summarized in Table III for the baseline DLR-F6 and in Table IV for the FX2B configuration. (Recall that these tables omit all Medium-Fine data based on the Tinoco grids so that comparison across data blocks is more consistent.) The estimated continuum values in these tables are based on Fine/Medium mesh extrapolations. Of these twenty blocks of data, one did not provide the pressure and skin-friction parts of drag.

Table III: Case 1 DLR-F6 Data Extrapolated To Continuum.

Tag	α	C_D	$C_{D.PR}$	$C_{D.SF}$	C_M	$C_D - C_L^2/(\pi AR)$
A	0.0244	0.02686	0.01404	0.01283	-0.14617	0.01843
B	-0.0614	0.02846	0.01420	0.01425	-0.15065	0.02005
C	0.1518	0.02613	0.01428	0.01185	-0.13747	0.01778
D	-0.0990	0.02732	0.01470	0.01261	-0.15342	0.01894
E	0.1824	0.02761	0.01552	0.01209	-0.14624	0.01930
F	0.2003	0.02772	0.01564	0.01208	-0.14602	0.01941
G	-0.1633	0.02622	0.01392	0.01231	-0.15753	0.01784
H	0.0472	0.02641	0.01438	0.01203	-0.14280	0.01803
I	-0.0909	0.02636	0.01402	0.01235	-0.14770	0.01799
J	0.0863	0.02658	0.01453	0.01205	-0.13211	0.01820
K	0.2692	0.02747	0.01544	0.01205	-0.13538	0.01910
L	0.0737	0.02695	0.01485	0.01210	-0.14450	0.01857
M	0.2663	0.02759	0.01561	0.01199	-0.13944	0.01923
N	0.1022	0.02612	0.01335	0.01252	-0.15245	0.01775
O	0.0400	0.02710	0.01375	0.01334	-0.16255	0.01844
P	1.2476	0.03226	0.02193	0.01035	-0.11064	0.02396
Q	0.1006	0.02626	0.01473	0.01151	-0.14349	0.01788
R	-1.1783	0.03325	-	-	-	0.02487
S	0.4938	0.02939	0.01740	0.01199	-0.12926	0.02101
Z	-0.1089	0.02846	0.01628	0.01215	-0.15433	0.02002

Table IV: Case 1 FX2B Data Extrapolated To Continuum.

Tag	α	C_D	$C_{D.PR}$	$C_{D.SF}$	C_M	$C_D - C_L^2/(\pi AR)$
A	0.1296	0.02701	0.01409	0.01293	-0.13977	0.01860
B	0.0950	0.02854	0.01430	0.01422	-0.14129	0.02013
C	0.2210	0.02639	0.01438	0.01199	-0.13328	0.01798
D	-0.1150	0.02705	0.01427	0.01275	-0.15310	0.01867
E	-0.0887	0.02628	0.01393	0.01235	-0.15479	0.01790
F	-0.0888	0.02628	0.01391	0.01237	-0.15489	0.01790
G	-0.0569	0.02624	0.01382	0.01244	-0.15189	0.01786
H	0.1178	0.02639	0.01423	0.01217	-0.13818	0.01802
I	-0.0673	0.02636	0.01388	0.01251	-0.14343	0.01798
J	0.1180	0.02655	0.01437	0.01220	-0.13562	0.01818
K	0.0507	0.02656	0.01438	0.01220	-0.14227	0.01818
L	0.0493	0.02643	0.01425	0.01220	-0.14353	0.01805
M	-0.0907	0.02596	0.01366	0.01230	-0.14997	0.01759
N	-0.1414	0.02527	0.01324	0.01202	-0.16042	0.01691
O	0.1570	0.02727	0.01472	0.01255	-0.13316	0.01875
P	0.3866	0.02584	0.01505	0.01077	-0.11826	0.01746
Q	0.2634	0.02606	0.01444	0.01161	-0.13338	0.01768
R	-0.0405	0.02934	-	-	-	0.02097
S	0.1207	0.02795	0.01569	0.01226	-0.13778	0.01957
Z	-0.1140	0.02627	0.01397	0.01228	-0.15451	0.01789

Figure 9 provides the Richardson-extrapolated absolute drag coefficients for the CFD results given in Tables III-IV, and NTF data from Eqn (4). In this bar chart, the baseline DLR-F6 drag coefficients are depicted in blue, while those of the FX2B configuration are shown in maroon. Note that on the extremes, data block C indicates a 2.6-count penalty, while data block P predicts a 64.2-count improvement. However, the DPW-III summary paper[38] identified data blocks A, B, C, P, R, S, and Z as outliers. Omitting these outlier data blocks, this range reduces to a 1.7-count penalty from data block O, and a 16.3-count improvement per data block M. Of the remaining data blocks, the average effect of the fairing is a 5.4-count reduction, with a standard deviation of 6.2 counts. Note that this delta drag improvement and scatter are about twice that of the published NTF data.

Figure 10 illustrates the size and location of the side-of-body separation bubble for the baseline DLR-F6 wing/body configuration, as computed by the participants. The air flow is from left to right, the bright vertical edge is the wing trailing edge, while the bright horizontal line approximates the wing/body intersection. The A-Z symbols plotted in this figure represent the (X-EYE,Y-EDGE) coordinates of the computed separation bubbles. Here, X-EYE depicts the streamwise position of the bubble eye (which is approximately the streamwise location of the maximum bubble width), and Y-EDGE is the maximum spanwise extent of the bubble. For reference, these data are overlayed on an oil-flow pattern taken from the NTF wind-tunnel test. For clarity, these data are organized into three subplots by grid type. This figure illustrates that there is large scatter in the computed sizes of the separation bubble, represented by Y-EDGE, even within the common grid types. A more global view of the oil-flow is provided in Figures 11-12. We note here that the width of this bubble is approximately the same as that from a previous ONERA wind-tunnel test, while the length of the NTF bubble is about twice that of the ONERA test; however, the Reynolds number of the ONERA test was 3 *million* instead of 5 *million*.

A couple of observations are noted; there are a few back-to-back comparisons in the data where only one variable changed. For example, the drag predicted using the full Navier-Stokes equations appears to be higher than that obtained using the thin-layer approximations. The back-to-back comparisons yielding this observation come from the data block pairs of (G,I), (H,J), and (L,K) for both the DLR-F6 and FX2B results; all six pairs exhibit this trend.

Another comparison that can be made is regarding the SA and SST turbulence models. Here refer to the data block pairs of (G,H), (I,J), and (M,U). Although we do not have sufficient data for a continuum estimate of the U data block, we can compare the DLR-F6 Medium grid results with those of the M data block. In this comparison, all five pairs of data show that the total drag from the SST model is higher than that from the SA model. Digging further into this SA/SST comparison shows that the pressure drag of the SST model is always higher than that of the SA model, yet the skin-friction drag shows the opposite trend in all cases.

In addition to the above trends identified, other trends have been investigated by participants of the DPW-III with post-workshop studies. As an example, Sclafani *et al.*[36] have studied the effect of an extreme refinement of the grid near the wing trailing edge. They also added an Extra-Fine mesh to their overset grid families; the results on the baseline DLR-F6 show that the side-of-body bubble monotonically grows with increasing grid refinement. Further, the size of the bubble is consistently larger when the flow is computed with the full Navier-Stokes equations as compared with that of the thin-layer approximations.

Case 1b: Drag Polar on Medium Grid Study

The remainder of this subsection provides the alpha-sweep data. For the sake of clarity, these data are presented by grid type using similar side-by-side plots as before, with DLR-F6 on the left and FX2B on the right. The NTF data are included with scatter bars for comparison.

Figures 13-16 provide idealized profile drag polars, comparing the NTF experimental data with the CFD results. Figure 13 is a composite plot of all of the CFD results, while the following plots break out this comparison by grid type.

Figure 14 provides the idealized profile drag of the data blocks based on multiblock structured grids. Note that these curves have been further itemized by grid family sets. The solid lines represent results using the Tinoco grid families; the dashed lines capture the Gridgen families; the chain-dot lines refer to the SAUNA grid families. In these figures, data block B appears to be an outlier related to the idealized profile drag, and data block A looks like an outlier with respect to skin friction. Both of these data blocks were identified as outliers by the filtering process of Vassberg *et al.*[38] In addition to these, the C data block was also identified as an outlier; based on this figure, the C data block appears to be on the fringe of the range of drag polars.

Figure 15 provides drag-polar results based on the overset mesh family. In this figure, it is interesting that the CFD did a better job of predicting the shape of the drag polar for the baseline DLR-F6 WB than it did for the FX2B configuration, especially for $C_L \geq 0.30$. In general this trend is not the case for the other CFD solutions, with the exception of the structured-mesh results based on Grid Set 2 (Figure 14).

Figure 16 addresses the unstructured and hybrid mesh data. These data are also grouped. The solid lines represent results based on the LaRC grid families; the dashed lines depict results using the AFLR grid families; the chain-dot lines capture data based on the five remaining unstructured-mesh families. The DLR-F6 idealized profile drag polar of data block P is dramatically rotated with respect to the general trend. Data block S resides at the extreme of scatter on both polars. The filter identified P and S as outliers; the W data block had insufficient grid-convergence data to be analyzed.

For completeness, lift and pitching moment curves are included next. Figure 17 shows the lift curves. In general, the CFD over predicts the lift relative to the experimental NTF data. The one CFD solution set (data block P) that came close to matching the NTF curve was identified as an outlier in the DPW-III summary paper.[38] Figure 18 shows the pitching moment curves. Here, most of the CFD results exhibit a more nose-down pitching moment than that of the NTF experimental data. (Note that the P and S data blocks were previously identified as outliers.) The computational results presented herein have utilized a rigid geometry that was defined to match the estimated shape at the design condition. The experimental data were collected with a geometry that flexes differently as the load changes during the alpha sweeps. The NTF data hints at a possible explanation for both of these discrepancies. Figure 19 illustrates that these NTF test data are consistent with the previously acquired lift and moment curves from ONERA, albiet that the data were collected at different Reynolds numbers. However, two new pieces of data might be instrumental in improving the understanding of the discrepancy between experiment and CFD. In the NTF test a full sectional pressure measurement was available at the outboard most wing station. Previously only pressures from the upper surface at this span station had been released. With this full sectional pressure distribution it is possible to calculate the local sectional lift distribution across the span of the model. A comparison of the predicted and measured lift distribution across the span is shown in Figure 20. In this figure, the Zeus/CFL3D solution of data block H (solid line) was calculated matching total lift. Note that the computational results predict lower lift on the inboard part of the wing and higher on the outboard part. If the CFD lift distribution is scaled to match the values at the inboard part of the wing (dashed line) we see that the predicted section lift is increasingly higher than the measured values as the span station increases. This indicates that the wing twist of the computational model may not match the twist of the model during the test at this flight condition. Washing out the wing twist will require running at a higher angle of attack for the same lift. Furthermore, since the CFD results predict a higher outboard loading than seen in the experimental data, this can also explain why the CFD predicts a more nose-down pitching moment for the swept-back wing of the DLR-F6 configuration. Validation requires adequate knowledge of the shape of the configuration under the flight conditions being compared. Wing twist and deflection measurements were taken during the NASA test. These data are still being processed and are not available at the time of this writing. While we still cannot fully explain the discrepancy in the comparison we now have data that suggests the wing geometry being modeled (specifically wing twist) does not correspond to that being tested. Better knowledge of the geometry being tested may help resolve this issue. Additional discussion addressing this discrepancy is provided by Tinoco.[48]

General Observation of the CFD Results

A general observation, after reviewing all of the results, is that there is a set of CFD codes whose members all seem to agree relatively well with each other, and do so over all of the test cases spanning the DPW Series. Most noteworthy about this core set of codes is that it is comprised of flow solvers that are based on all types of grids.

VI.   On-Going Plans

Planning for the Fourth AIAA Drag Prediction Workshop (DPW-IV) is underway. DPW-IV will be held June 2009 in San Antonio, TX in conjunction with the 27th AIAA Applied Aerodynamics Conference. The emphasis of DPW-IV is related to the prediction of drag with a configuration in static trim. The purpose of focusing on this problem is to introduce incremental pitching-moment calculations into the database of CFD predictions for code validations. As with DPW-III, the test cases of DPW-IV will be *blind* predictions, in

that no relevant experimental data will be available prior to the workshop. The DPW-IV subject geometry is the wing-body-horizonal tail configuration of the NASA Common Research Model (CRM), which is also the product of an on-going collaboration between US Aircraft Industry and NASA. The current status of the design, fabrication, and experimental test plans for the CRM is outlined in Vassberg *et al.*[49] The analytic geometry definition for the wing-body-horizontal tail configuration will be made available to the public domain on the DPW-IV website by August 2008. Construction of the DPW-IV baseline grids are pending the CRM geometry release, but will begin immediately thereafter. For further updates on schedule and baseline grid availability, please refer to the DPW-IV website.[50]

VII.   Conclusions

Experimental data on the DLR-F6 wing-body configuration from the National Transonic Facility (NTF) are compared with predictions from the Third AIAA Drag Prediction Workshop (DPW-III); these predictions were published prior to the existance of corresponding experimental data. An analysis of the experimental data is included to help assess the drag of the DLR-F6 WB with and without the FX2B fairing at $M = 0.75$ and $Re = 5 \ million$. These curve fits of the NTF data are also used to estimate the incremental drag effect of the FX2B fairing at the design lift condition of $C_L = 0.50$.

DPW-III focused on the prediction of drag for wing-body and wing-alone configurations that are representative of transonic transport aircraft. Numerical calculations were performed using industry-relevant test cases. Numerous Reynolds-Averaged Navier-Stokes CFD results on fully-turbulent flows are provided. These solutions are performed on structured, unstructured, and hybrid grid systems. The structured grid sets include point-matched multi-block meshes and over-set grid systems. The unstructured and hybrid grid sets are comprised of tetrahedral, pyramid, and prismatic elements. Effort was made to provide a high-quality and parametrically consistent family of grids for each grid type about each configuration under study. The wing-body families are comprised of coarse, medium, and fine grids. These mesh sequences are utilized to help determine how the provided flow solutions fare with respect to asymptotic grid convergence, and are used to estimate an absolute drag of each configuration.

Comparing the experimental data from the NTF wind-tunnel test with the database of CFD results from DPW-III indicates that additional effort will be required before these two sources of aerodynamic performance assessment sufficiently match each other. In general, even the incremental drag effect of the FX2B fairing is not well predicted by CFD with respect to the NTF. Only a third of the submissions yielded a consistent delta drag, while the average increment was about twice that of the NTF data. However, some insight into these discrepancies may have been identified by analyzing the spanload distributions of the NTF data, which could partially explain differences in both the lift and pitching-moment levels between experiment and simulation.

The DPW Series has provided a very broad view of the state-of-the-art of CFD applications within the industry, much more so than that which can be garnered by an isolated study. In fact, by reviewing in isolation any one of the DPW-III's individual data blocks, one may arrive at different conclusions than those presented herein. For example, a typical publication may show how successful a CFD solution matches test data. By combining a large set of solutions from many sources around the world, this workshop clearly shows that there remains much room for improvement. While this conclusion is somewhat disappointing, it is tempered by an observation that there exists a core set of CFD methods that consistently agree with each other in general, and do so on all test cases spanning the workshop series. Most noteworthy about this core set of solvers is that these methods are based on all grid types.

Through the data compiled by this workshop, it is obvious that several problematic issues continue to persist in the processes used for accurate drag prediction. Generating a consistent set of grids for the purpose of grid-convergence studies remains a challenge, especially for unstructured meshes. The side-of-body separation bubble of the DLR-F6 wing/body configuration continues to be a source of difficulty; the full set of CFD solutions show a large variation of predicted bubble sizes. However, on a good note, the skin-friction predictions of the aggregate data blocks are well behaved and form relatively tight groupings.

VIII.   Acknowledgments

References

[1] 1st AIAA CFD Drag Prediction Workshop. http://aaac.larc.nasa.gov/tsab/cfdlarc/aiaa−dpw/Workshop1/workshop1.html, dpw@cessna.textron.com, Anaheim, CA, June 2001.

[2] G. Redeker. DLR-F4 wing-body configuration. In *A Selection of Experimental Test Cases for the Validation of CFD Codes*, number *AR-303*, pages B4.1–B4.21. AGARD, August 1994.

[3] J. C. Vassberg, M. A. DeHaan, and A. J. Sclafani. Grid generation requirements for accurate drag predictions based on OVERFLOW calculations. *AIAA Paper 2003-4124*, 16th AIAA Computational Fluid Dynamics Conference, Orlando, FL, June 2003.

[4] D. W. Levy, J. C. Vassberg, R. A. Wahls, T. Zickuhr, S. Agrawal, S. Pirzadeh, and M. J. Hemsch. Summary of data from the first AIAA CFD Drag Prediction Workshop. *AIAA paper 2002-0841*, 40th AIAA Aerospace Sciences Meeting & Exhibit, Reno, NV, January 2002.

[5] D. W. Levy, J. C. Vassberg, R. A. Wahls, T. Zickuhr, S. Agrawal, S. Pirzadeh, and M. J. Hemsch. Summary of data from the first AIAA CFD Drag Prediction Workshop. *AIAA Journal of Aircraft*, 40(5):875–882, Sep–Oct 2003.

[6] M. J. Hemsch. Statistical analysis of CFD solutions from the Drag Prediction Workshop. *AIAA paper 2002-0842*, 40th AIAA Aerospace Sciences Meeting & Exhibit, Reno, NV, January 2002.

[7] M. Hemsch. Statistical analysis of CFD solutions from the drag prediction workshops. In *CFD-based Aircraft Drag Prediction and Reduction*, Hampton, VA, November 2003. von Karman Institue Lecture Series.

[8] M. Rakowitz, B. Eisfeld, D. Schwamborn, and M. Sutcliffe. Structured and unstructured computations on the DLR-F4 wing-body configuration. *AIAA paper 2002-0837*, 40th AIAA Aerospace Sciences Meeting & Exhibit, Reno, NV, January 2002.

[9] M. Rakowitz, B. Eisfeld, D. Schwamborn, and M. Sutcliffe. Structured and unstructured computations on the DLR-F4 wing-body configuration. *AIAA Journal of Aircraft*, 40(2):256–264, 2003.

[10] D. J. Mavriplis and D. W. Levy. Transonic drag predictions using an unstructured multigrid solver. *AIAA paper 2002-0838*, 40th AIAA Aerospace Sciences Meeting & Exhibit, Reno, NV, January 2002.

[11] S. Z. Pirzadeh and N. T. Frink. Assessment of the unstructured grid software TetrUSS for drag prediction of the DLR-F4 configuration. *AIAA paper 2002-0839*, 40th AIAA Aerospace Sciences Meeting & Exhibit, Reno, NV, January 2002.

[12] J. C. Vassberg, P. G. Buning, and C. L. Rumsey. Drag prediction for the DLR-F4 wing/body using OVERFLOW and CFL-3D on an overset mesh. *AIAA Paper 2002-0840*, 40th AIAA Aerospace Sciences Meeting & Exhibit, Reno, NV, January 2002.

[13] 2nd AIAA CFD Drag Prediction Workshop. http://aaac.larc.nasa.gov/tsab/cfdlarc/aiaa−dpw/Workshop2/workshop2.html, dpw@cessna.textron.com, Orlando, FL, June 2003.

[14] K. R. Laflin, J. C. Vassberg, R. A. Wahls, J. H. Morrison, O. Brodersen, M. Rakowitz, E. N. Tinoco, and J. Godard. Summary of data from the second AIAA CFD drag prediction workshop. *AIAA Paper 2004-0555*, 42nd AIAA Aerospace Sciences Meeting and Exhibit, Reno, NV, January 2004.

[15] K. R. Laflin, J. C. Vassberg, R. A. Wahls, J. H. Morrison, O. Brodersen, M. Rakowitz, E. N. Tinoco, and J. Godard. Summary of data from the second AIAA CFD drag prediction workshop. *AIAA Journal of Aircraft*, 42(5):1165–1178, 2005.

[16] M. Hemsch and J. Morrison. Statistical analysis of CFD solutions from 2nd drag prediction workshop. *AIAA Paper 2004-0556*, 42nd AIAA Aerospace Sciences Meeting and Exhibit, Reno, NV, January 2004.

[17] N. Pfeiffer. Reflections on the second drag prediction workshop. *AIAA Paper 2004-0557*, 42nd AIAA Aerospace Sciences Meeting and Exhibit, Reno, NV, January 2004.

[18] O. Brodersen, M. Rakowitz, S. Amant, P. Larrieu, D. Destarac, and M. Sutcliffe. Airbus, ONERA, and DLR results from the 2nd AIAA drag prediction workshop. *AIAA Paper 2004-0391*, 42nd AIAA Aerospace Sciences Meeting and Exhibit, Reno, NV, January 2004.

[19] O. P. Brodersen, M. Rakowitz, S. Amant, P. Larrieu, D. Destarac, and M. Suttcliffe. Airbus, ONERA and DLR results from the second AIAA drag prediction workshop. *AIAA Journal of Aircraft*, 42(4):932–940, 2005.

[20] R. B. Langtry, M. Kuntz, and F. Menter. Drag prediction of engine-airframe interference effects with CFX-5. *AIAA Paper 2004-0392*, 42nd AIAA Aerospace Sciences Meeting and Exhibit, Reno, NV, January 2004.

[21] R. B. Langtry, M. Kuntz, and F. Menter. Drag prediction of engine-airframe interference effects with CFX-5. *AIAA Journal of Aircraft*, 42(6):1523–1529, 2005.

[22]A. J. Sclafani, M. A. DeHaan, and J. C. Vassberg. OVERFLOW drag predictions for the DLR-F6 transport configuration: A DPW-II case study. *AIAA Paper 2004-0393*, 42nd AIAA Aerospace Sciences Meeting and Exhibit, Reno, NV, January 2004.

[23]C. Rumsey, M. Rivers, and J. Morrison. Study of CFD variations on transport configurations from the 2nd AIAA drag prediction workshop. *AIAA Paper 2004-0394*, 42nd AIAA Aerospace Sciences Meeting and Exhibit, Reno, NV, January 2004.

[24]K. Wutzler. Aircraft drag prediction using Cobalt. *AIAA Paper 2004-0395*, 42nd AIAA Aerospace Sciences Meeting and Exhibit, Reno, NV, January 2004.

[25]G. May, E. van der Weide, A. Jameson, and S. Shankaran. Drag prediction of the DLR-F6 configuration. *AIAA Paper 2004-0396*, 42nd AIAA Aerospace Sciences Meeting and Exhibit, Reno, NV, January 2004.

[26]Y. Kim, S. Park, and J. Kwon. Drag prediction of DLR-F6 using the turbulent Navier-Stokes calculations with multigrid. *AIAA Paper 2004-0397*, 42nd AIAA Aerospace Sciences Meeting and Exhibit, Reno, NV, January 2004.

[27]K. Yamamoto, A. Ochi, E. Shima, and R. Takaki. CFD sensitivity to drag prediction on DLR-F6 configuration by structured method and unstructured method. *AIAA Paper 2004-0398*, 42nd AIAA Aerospace Sciences Meeting and Exhibit, Reno, NV, January 2004.

[28]E. Tinoco and T. Su. Drag prediction with the Zeus/CFL3D system. *AIAA Paper 2004-0552*, 42nd AIAA Aerospace Sciences Meeting and Exhibit, Reno, NV, January 2004.

[29]S. Klausmeyer. Drag, lift, and moment estimates for transonic aircraft using the Navier-Stokes equations. *AIAA Paper 2004-0553*, 42nd AIAA Aerospace Sciences Meeting and Exhibit, Reno, NV, January 2004.

[30]E. Lee-Rausch, N. Frink, W. Milholen, and D. Mavriplis. Transonic drag prediction using unstructured grid solvers. *AIAA Paper 2004-0554*, 42nd AIAA Aerospace Sciences Meeting and Exhibit, Reno, NV, January 2004.

[31]3rd AIAA CFD Drag Prediction Workshop. http://aaac.larc.nasa.gov/tsab/cfdlarc/aiaa−dpw/Workshop3/workshop3.html, dpw@cessna.textron.com, San Francisco, CA, June 2006.

[32]J. C. Vassberg, A. J. Sclafani, and M. A. DeHaan. A wing-body fairing design for the DLR-F6 model: a DPW-III case study. *AIAA Paper 2005-4730*, AIAA 23rd Applied Aerodynamics Conference, Toronto, Canada, June 2005.

[33]J. H. Morrison and M. J. Hemsch. Statistical analysis of CFD solutions from the third AIAA drag prediction workshop. *AIAA Paper 2007-0254*, 45th AIAA Aerospace Sciences Meeting and Exhibit, Reno, NV, January 2007.

[34]E. N. Tinoco, C. Winkler, M. Mani, and V. Venkatakrishnan. Structured and unstructured solvers for the 3rd CFD drag prediction workshop. *AIAA Paper 2007-0255*, 45th AIAA Aerospace Sciences Meeting and Exhibit, Reno, NV, January 2007.

[35]D. J. Mavriplis. Results from the 3rd drag prediction workshop using the NSU3D unstructured mesh solver. *AIAA Paper 2007-0256*, 45th AIAA Aerospace Sciences Meeting and Exhibit, Reno, NV, January 2007.

[36]A. J. Sclafani, J. C. Vassberg, N. A. Harrison, M. A. DeHaan, C. L. Rumsey, S. M. Rivers, and J. H. Morrison. Drag predictions for the DLR-F6 wing/body and DPW wings using CFL3D and OVERFLOW on an overset mesh. *AIAA Paper 2007-0257*, 45th AIAA Aerospace Sciences Meeting and Exhibit, Reno, NV, January 2007.

[37]O. Brodersen, B. Eisfeld, J. Raddatz, and P. Frohnapfel. DLR results from the third AIAA CFD drag prediction workshop. *AIAA Paper 2007-0259*, 45th AIAA Aerospace Sciences Meeting and Exhibit, Reno, NV, January 2007.

[38]J. C. Vassberg, E. N. Tinoco, M. Mani, O. P. Brodersen, B. Eisfeld, R. A. Wahls, J. H. Morrison, T. Zickuhr, K. R. Laflin, and D. J. Mavriplis. Summary of the third AIAA CFD drag prediction workshop. *AIAA Paper 2007-0260*, 45th AIAA Aerospace Sciences Meeting and Exhibit, Reno, NV, January 2007.

[39]E. N. Tinoco, V. Venkatakrishnan, C. Winkler, and M. Mani. Structured and unstructured solvers for the third AIAA CFD drag prediction workshop. *AIAA Journal of Aircraft*, 45(3):738–749, May–June 2008.

[40]D. J. Mavriplis. Third drag prediction workshop results using NSU3D unstructured mesh solver. *AIAA Journal of Aircraft*, 45(3):750–761, May–June 2008.

[41]A. J. Sclafani, J. C. Vassberg, N. A. Harrison, C. L. Rumsey, S. M. Rivers, and J. H. Morrison. CFL3D / OVERFLOW results for DLR-F6 wing/body and drag prediction workshop wing. *AIAA Journal of Aircraft*, 45(3):762–780, May–June 2008.

[42]J. C. Vassberg, E. N. Tinoco, M. Mani, O. P. Brodersen, B. Eisfeld, R. A. Wahls, J. H. Morrison, T. Zickuhr, K. R. Laflin, and D. J. Mavriplis. Abridged summary of the third AIAA CFD drag prediction workshop. *AIAA Journal of Aircraft*, 45(3):781–798, May–June 2008.

[43]M. Murayama and K. Yamamoto. DLR results from the third AIAA computational fluid dynamics drag prediction workshop. *AIAA Journal of Aircraft*, 45(3):823–836, May–June 2008.

[44]P. Eliasson and S.-H. Peng. Drag prediction for the DLR-F6 wing-body configuration using the Edge solver. *AIAA Journal of Aircraft*, 45(3):837–847, May–June 2008.

[45]G. M. Gatlin, S. M. Rivers, S. L. Goodliff, R. Rudnik, and M. Sitzmann. Experimental investigation of the DLR-F6 transport configuration in the National Transonic Facility. *AIAA Paper 2008-6917*, 26th AIAA Applied Aerodynamics Conference, Hawaii, HI, August 2008.

[46]A. W. Burner, W. K. Goad, E. A. Massey, L. R. Goad, S. L. Goodliff, and O. W. Bissett. Wing deformation measurements of the DLR-F6 transport configuration in the National Transonic Facility. *AIAA Paper 2008-6921*, 26th AIAA Applied Aerodynamics Conference, Hawaii, HI, August 2008.

[47]O. Brodersen and A. Sturmer. Drag prediction of engine-airframe interference effects using unstructured Navier-Stokes calculations. *AIAA Paper 2001-2414*, 19th AIAA Applied Aerodynamics Conference, Anaheim, CA, June 2001.

[48]E. N. Tinoco. Validation and minimizing CFD uncertainty for commercial aircraft applications. *AIAA Paper 2008-6902*, 26th AIAA Applied Aerodynamics Conference, Hawaii, HI, August 2008.

[49]J. C. Vassberg, M. A. DeHaan, S. M. Rivers, and R. A. Wahls. Development of a Common Research Model for applied CFD validation studies. *AIAA Paper 2008-6919*, 26th AIAA Applied Aerodynamics Conference, Hawaii, HI, August 2008.

[50]4th AIAA CFD Drag Prediction Workshop. http://aaac.larc.nasa.gov/tsab/cfdlarc/aiaa−dpw/, dpw@cessna.textron.com, San Antonio, TX, June 2009.
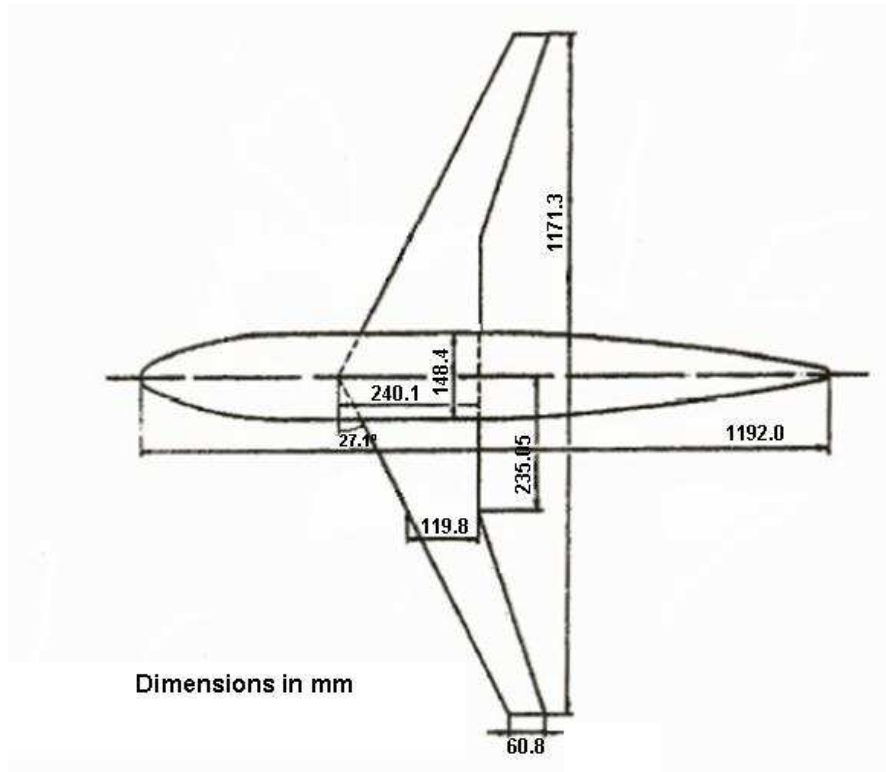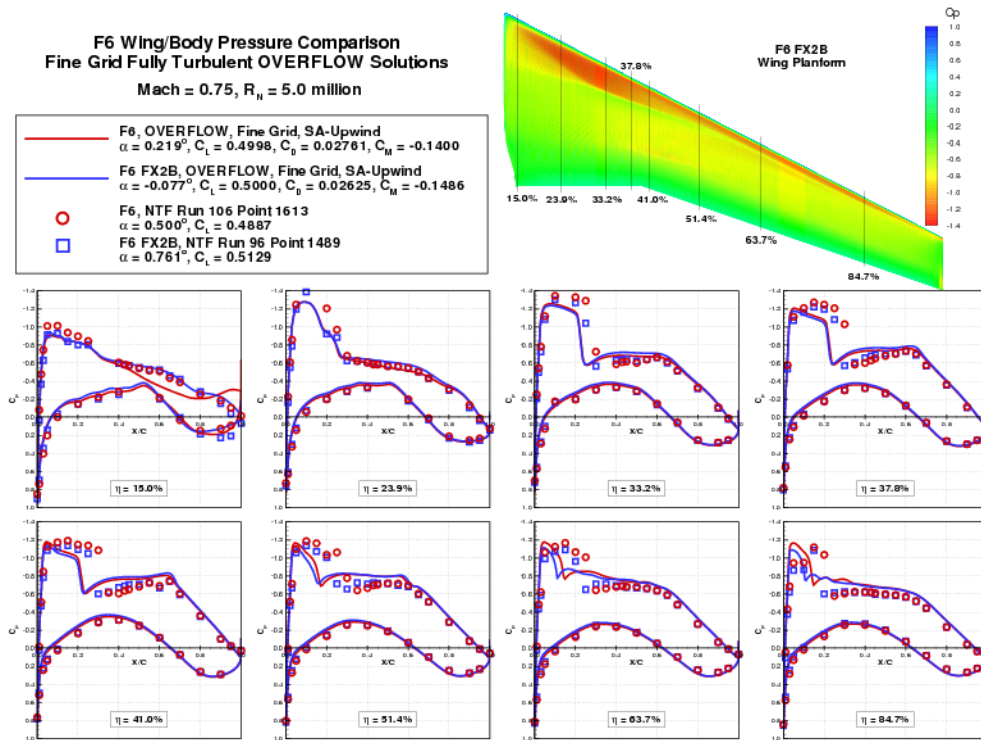
Figure 1. DLR-F6 Wing/Body Planform.

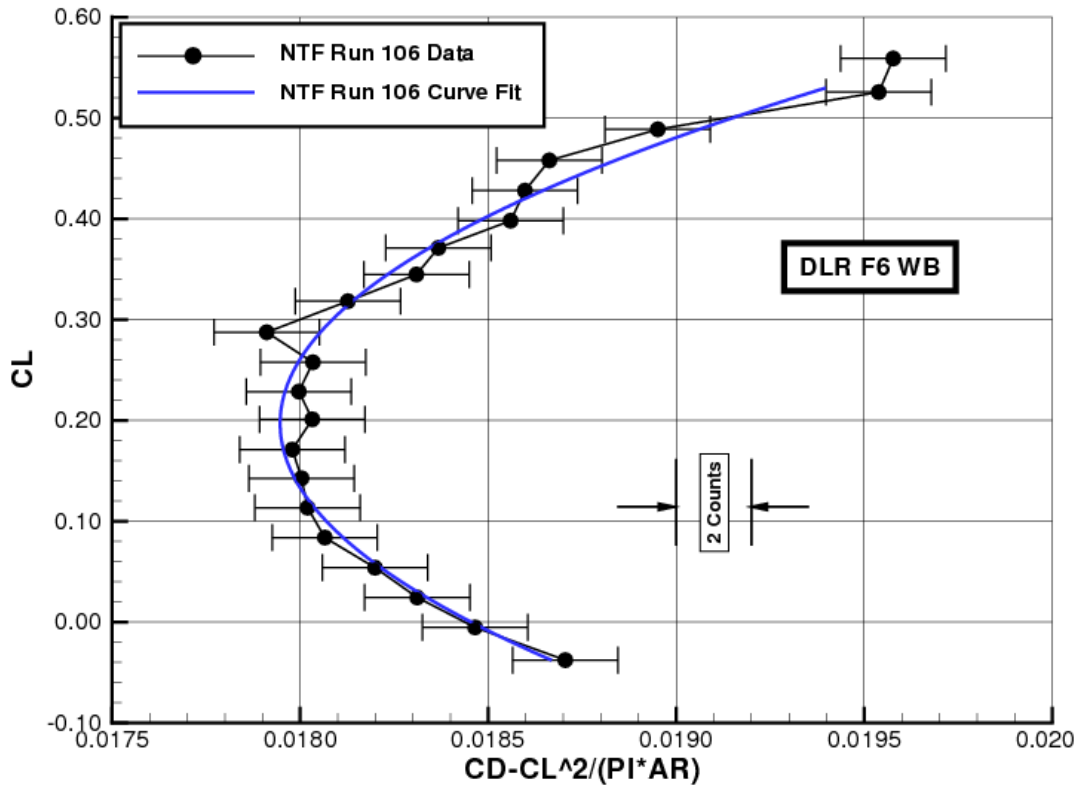Figure 2. Comparison of Pressure Distributions on the DLR-F6 Wing/Body: $M = 0.75$, $C_L = 0.5$, $Re = 5\ million$.

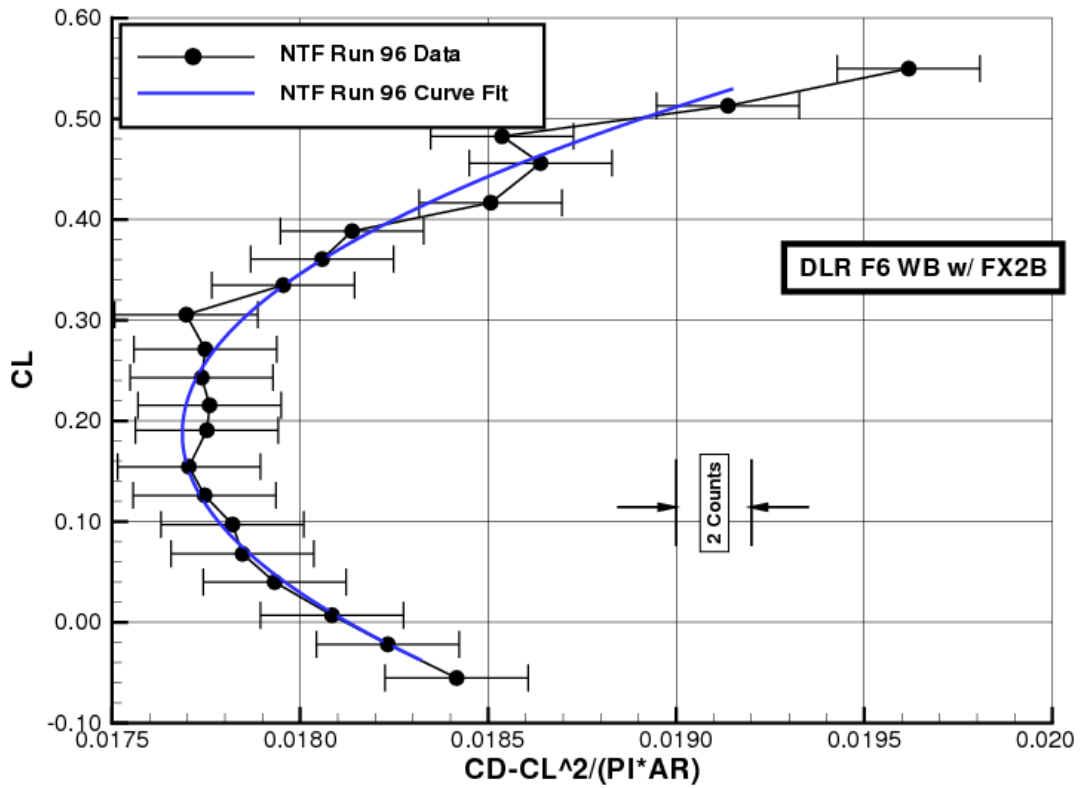**Figure 3. NTF DLR-F6 Idealized Profile Drag Polar:** $M = 0.75$, $Re = 5\ million$.

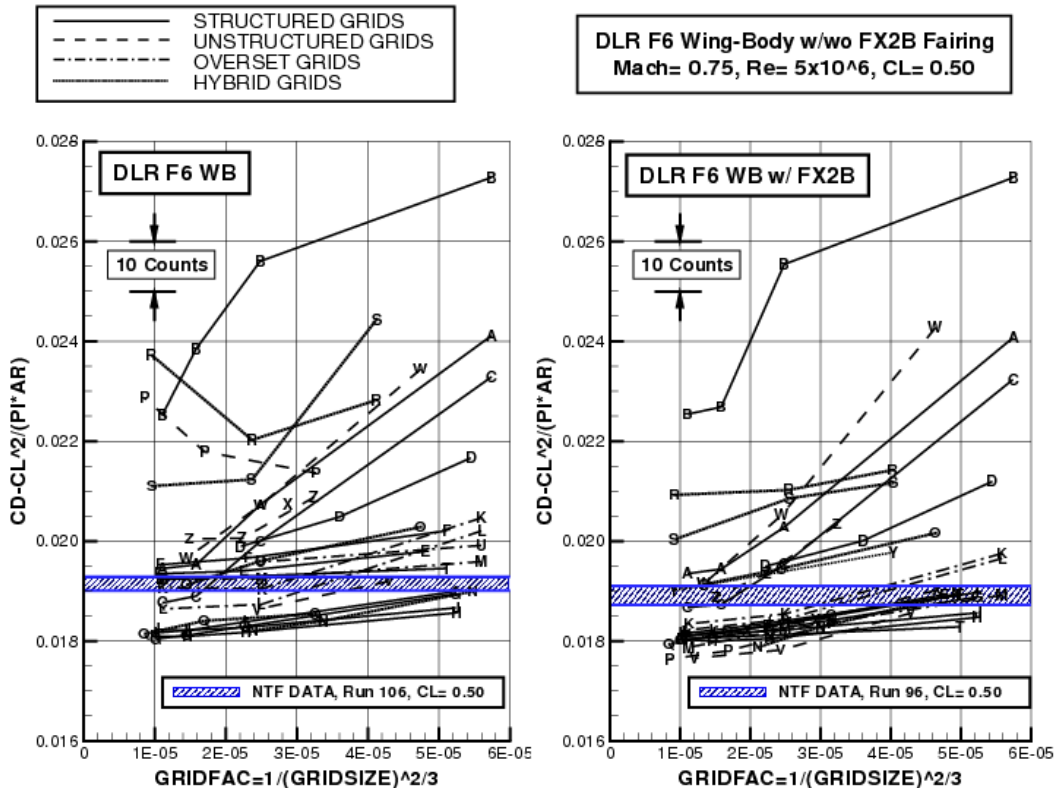**Figure 4. NTF FX2B Idealized Profile Drag Polar:** $M = 0.75$, $Re = 5\ million$.

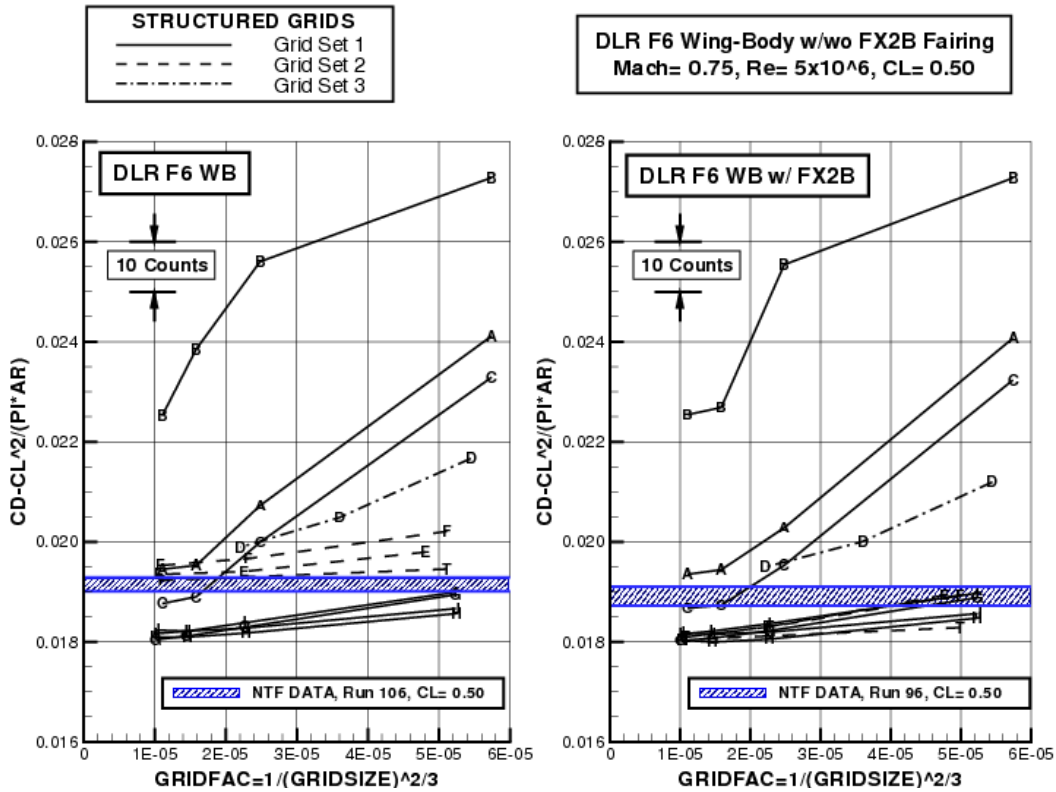Figure 5. Case 1 Grid Sensitivity on Idealized Profile Drag: $M = 0.75$, $C_L = 0.5$, $Re = 5\ million$.

Figure 6. Case 1 Grid Sensitivity on Structured Mesh Idealized Profile Drag.
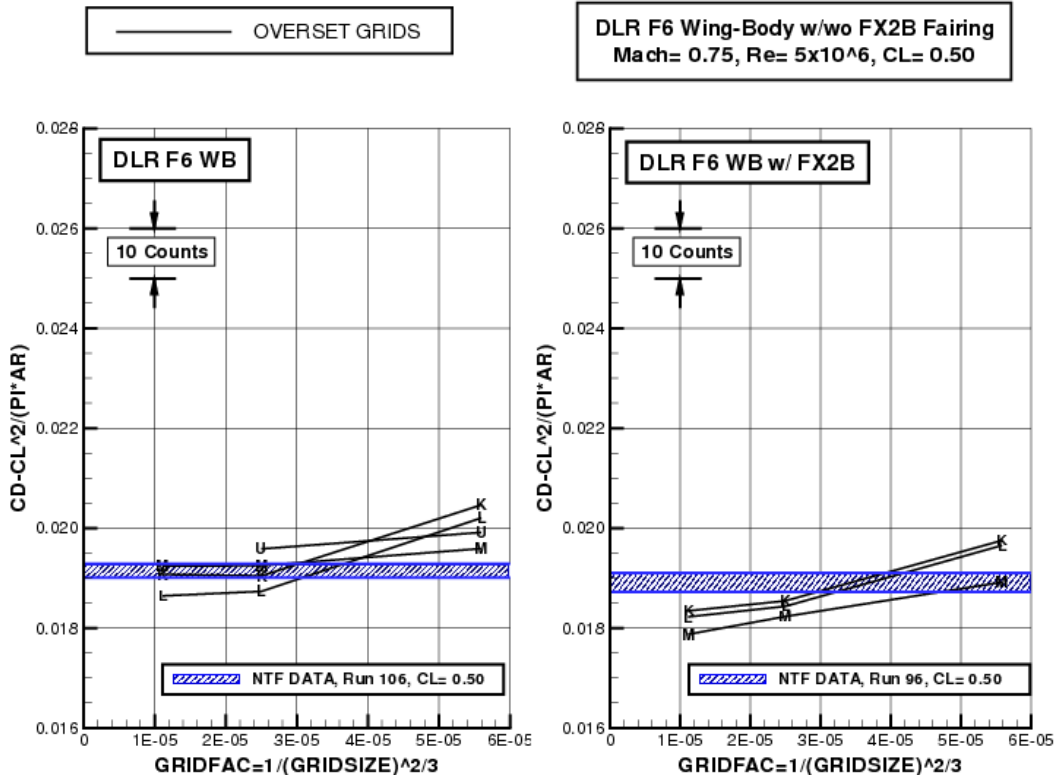
Figure 7. Case 1 Grid Sensitivity on Overset Mesh Idealized Profile Drag.
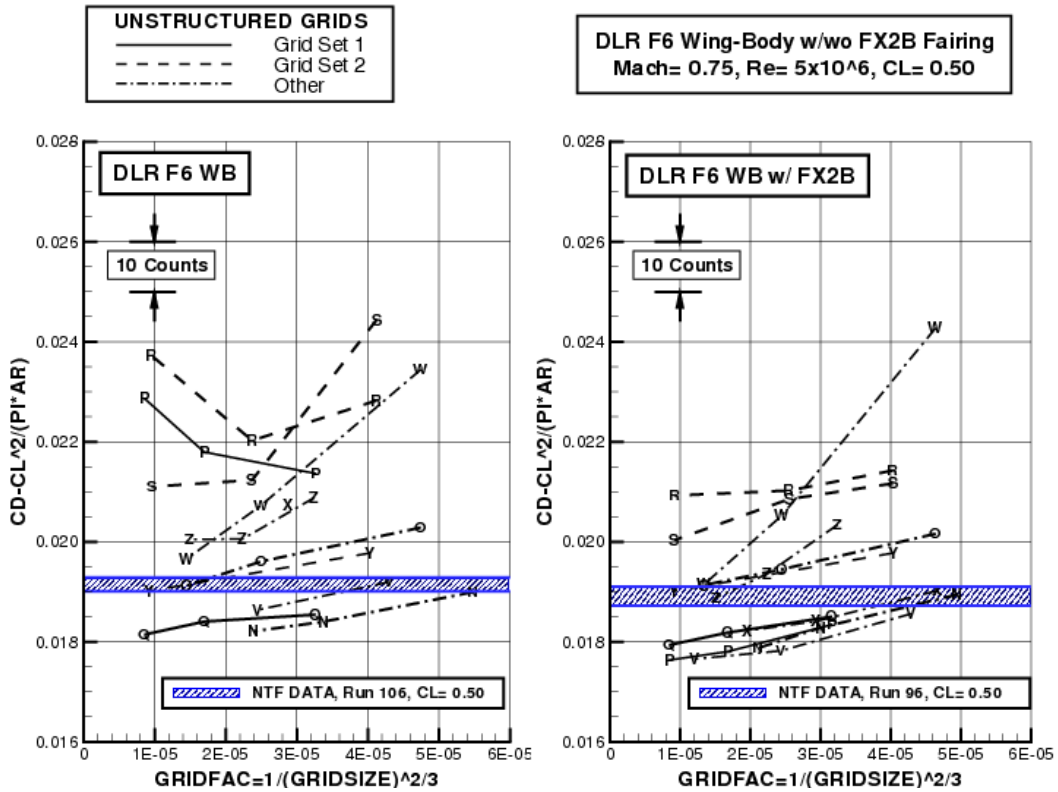
Figure 8. Case 1 Grid Sensitivity on Unstructured Mesh Idealized Profile Drag.

DLR-F6 Wing-Body Configuration
M=0.75 , Re=5M , CL=0.50
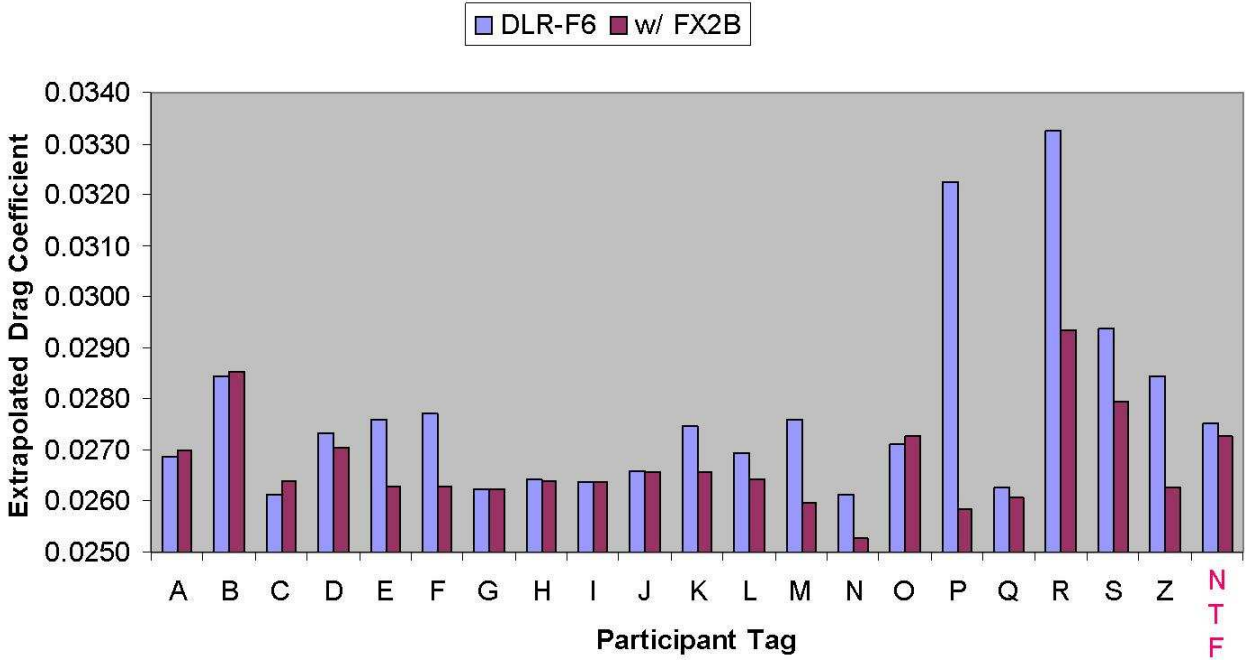
Figure 9. Case 1 Extrapolated Total Drag Coefficients.
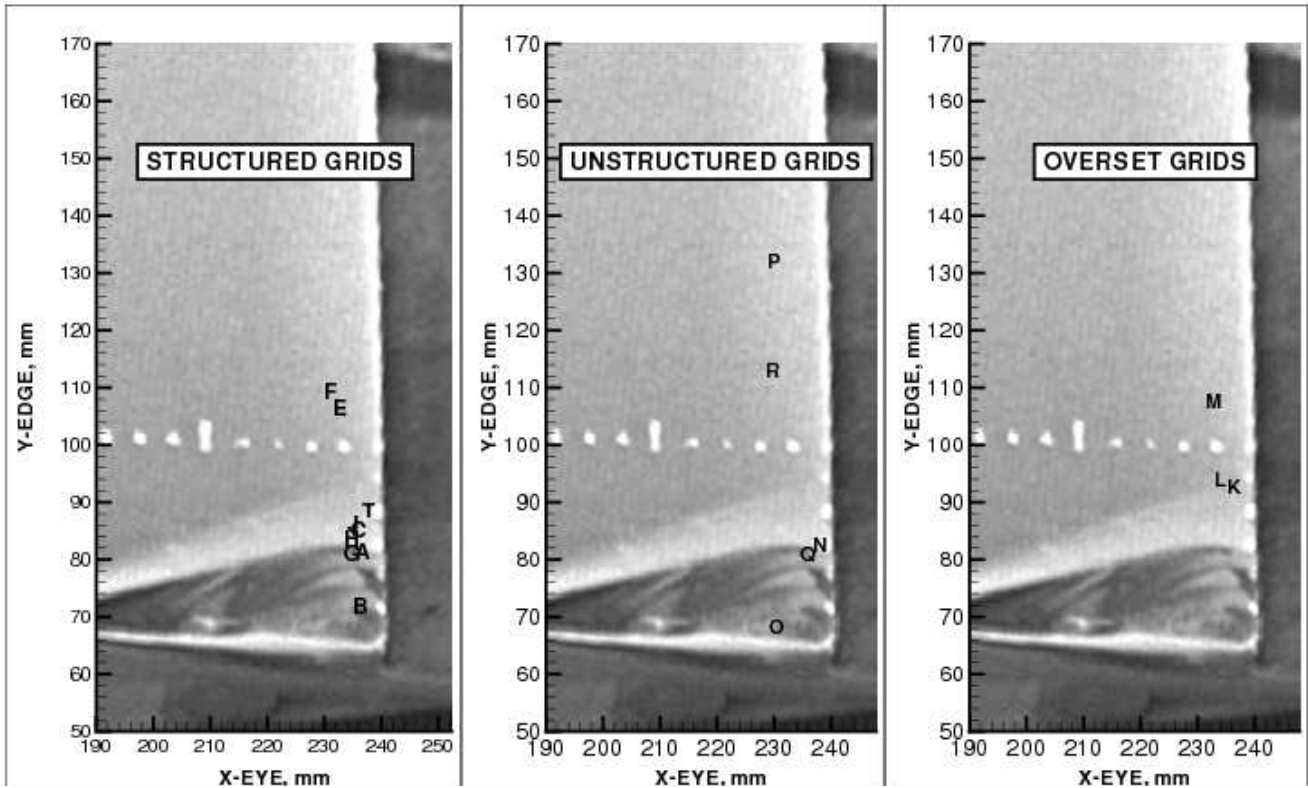
Figure 10. Case 1 Side-of-Body Separation Bubble Characteristics of the Baseline DLR-F6.
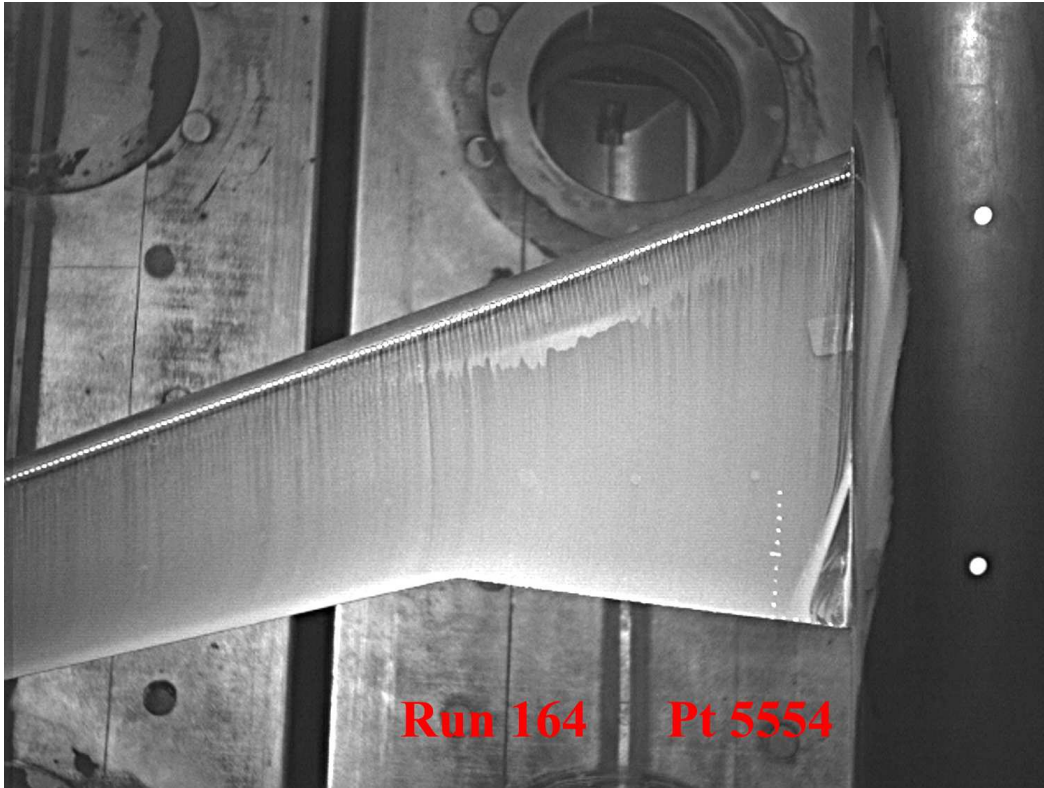
Figure 11. Side-of-Body Separation Bubble of the Baseline DLR-F6 in the NTF.
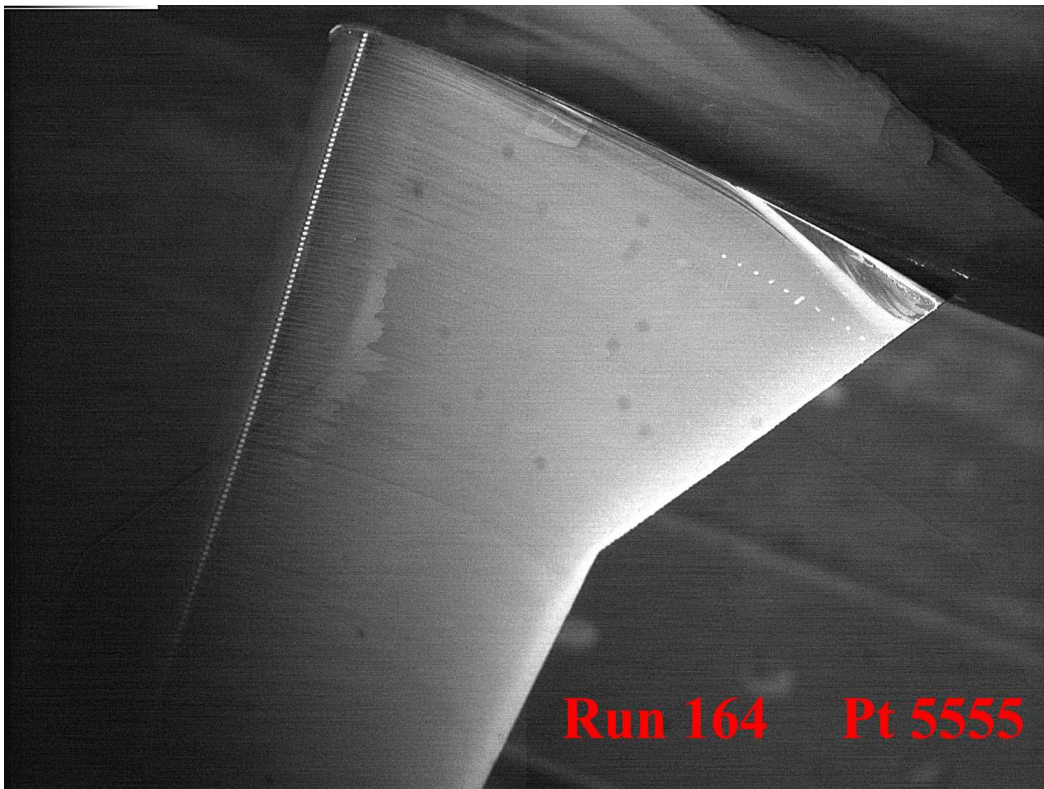
Figure 12. Side-of-Body Separation Bubble of the Baseline DLR-F6 in the NTF.
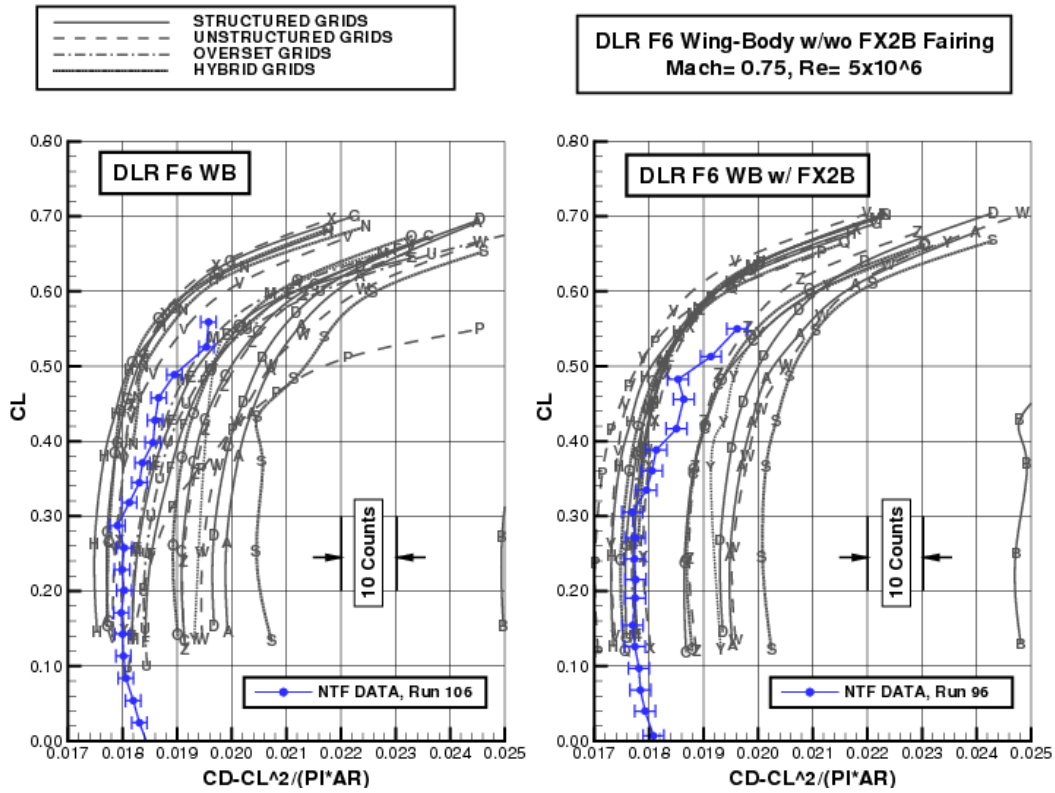
Figure 13. Case 1 Idealized Profile Drag Polars.
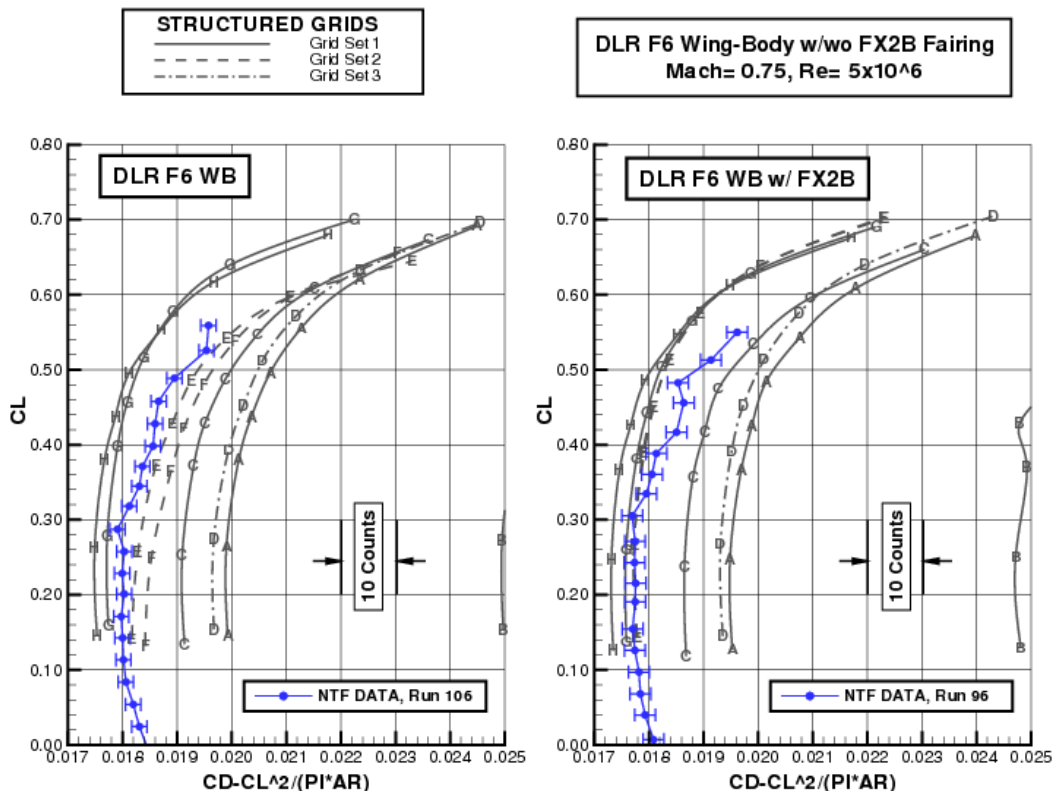
Figure 14. Case 1 Structured Mesh Idealized Drag Polars.
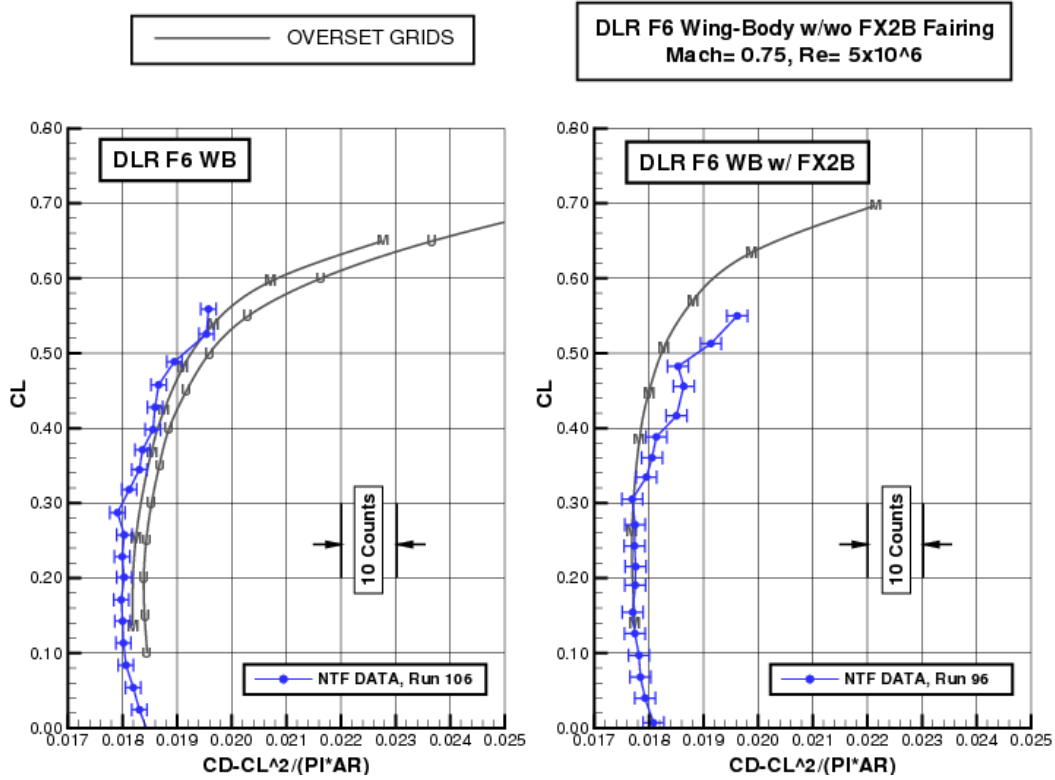
Figure 15. Case 1 Overset Mesh Idealized Profile Drag Polars.
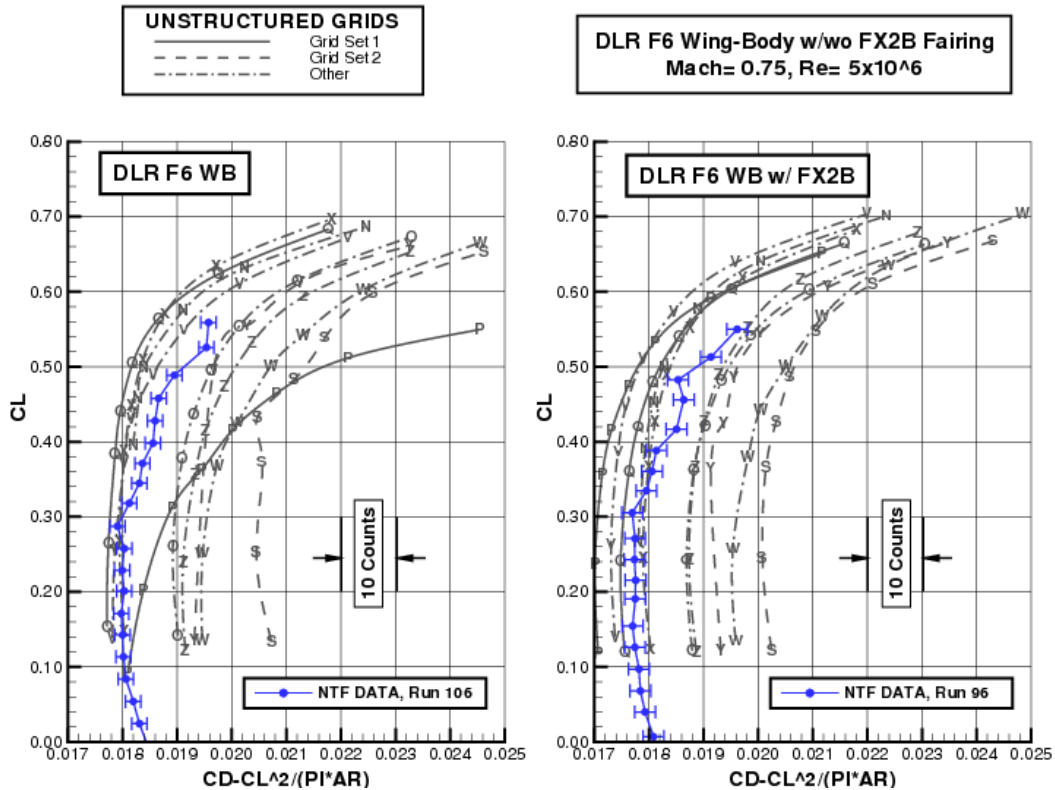
Figure 16. Case 1 Unstructured Mesh Idealized Profile Drag Polars.
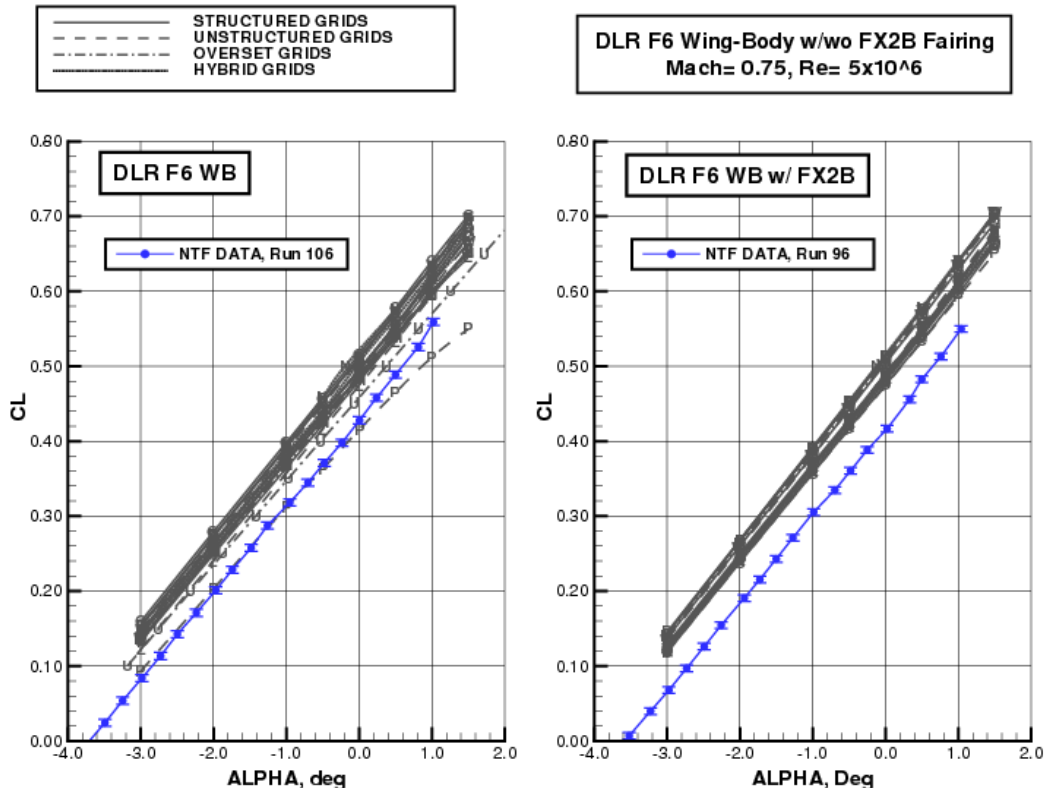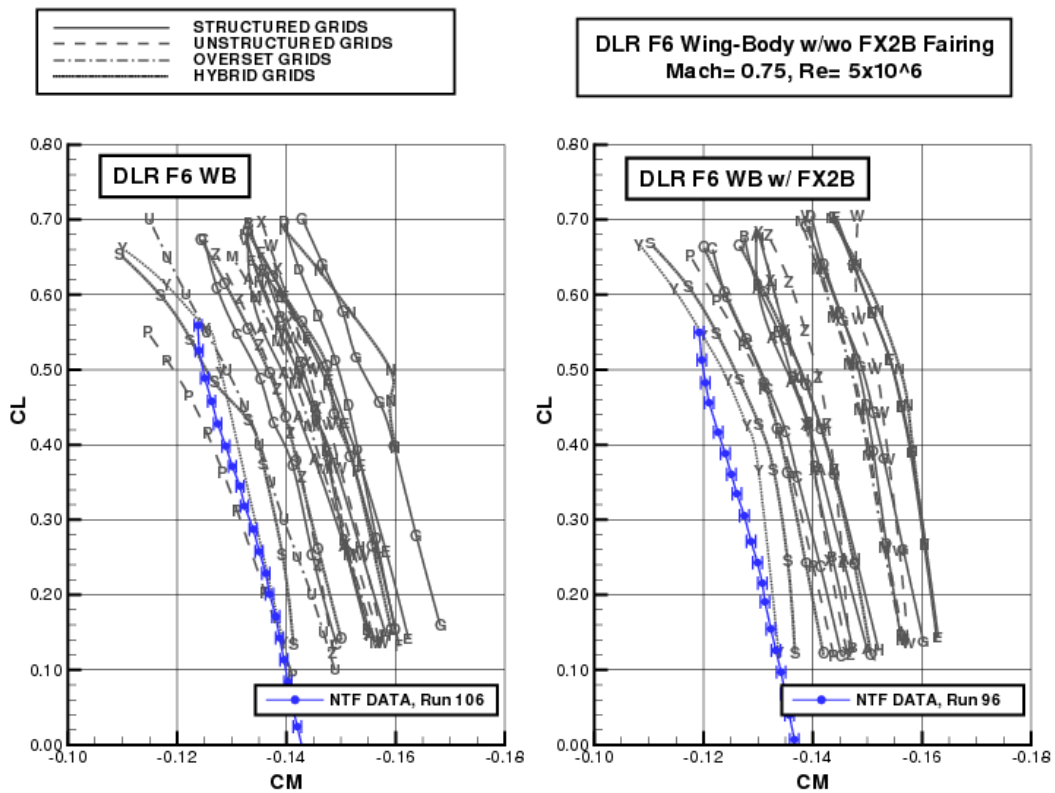
Figure 17. Case 1 Lift Curves.

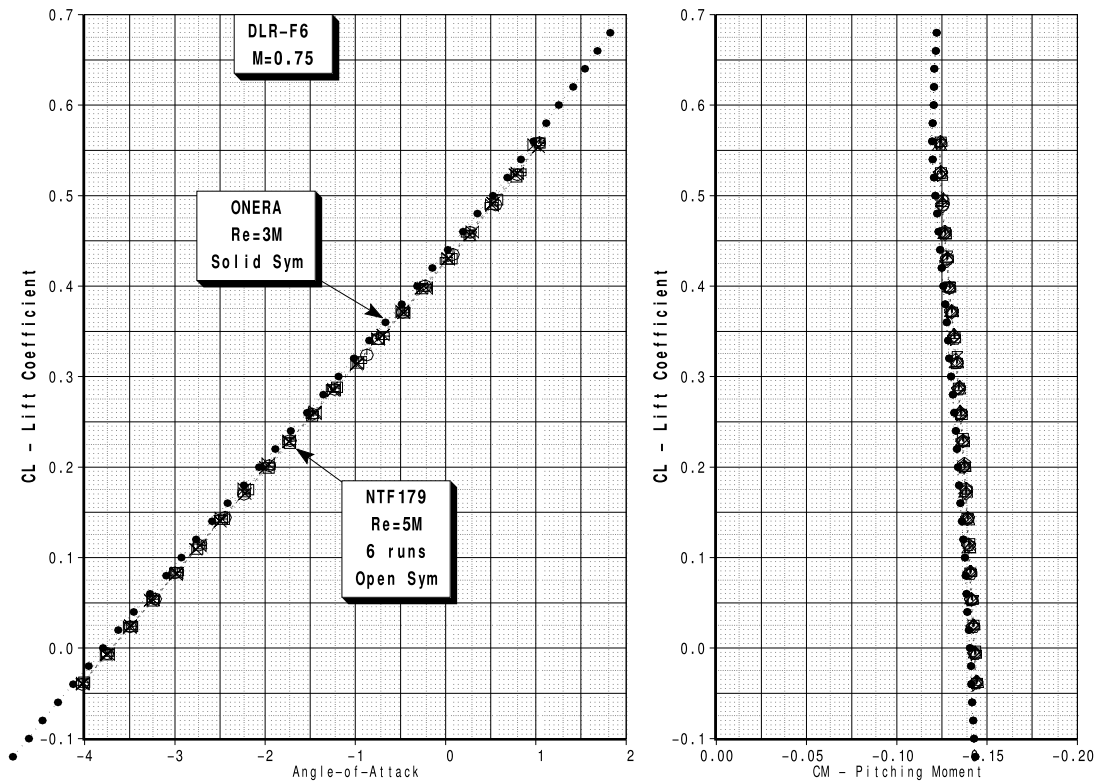Figure 18. Case 1 Pitching Moment Curves.

Figure 19. Comparison of NTF and ONERA WT Data of Lift and Pitching Moments for the DLR-F6.
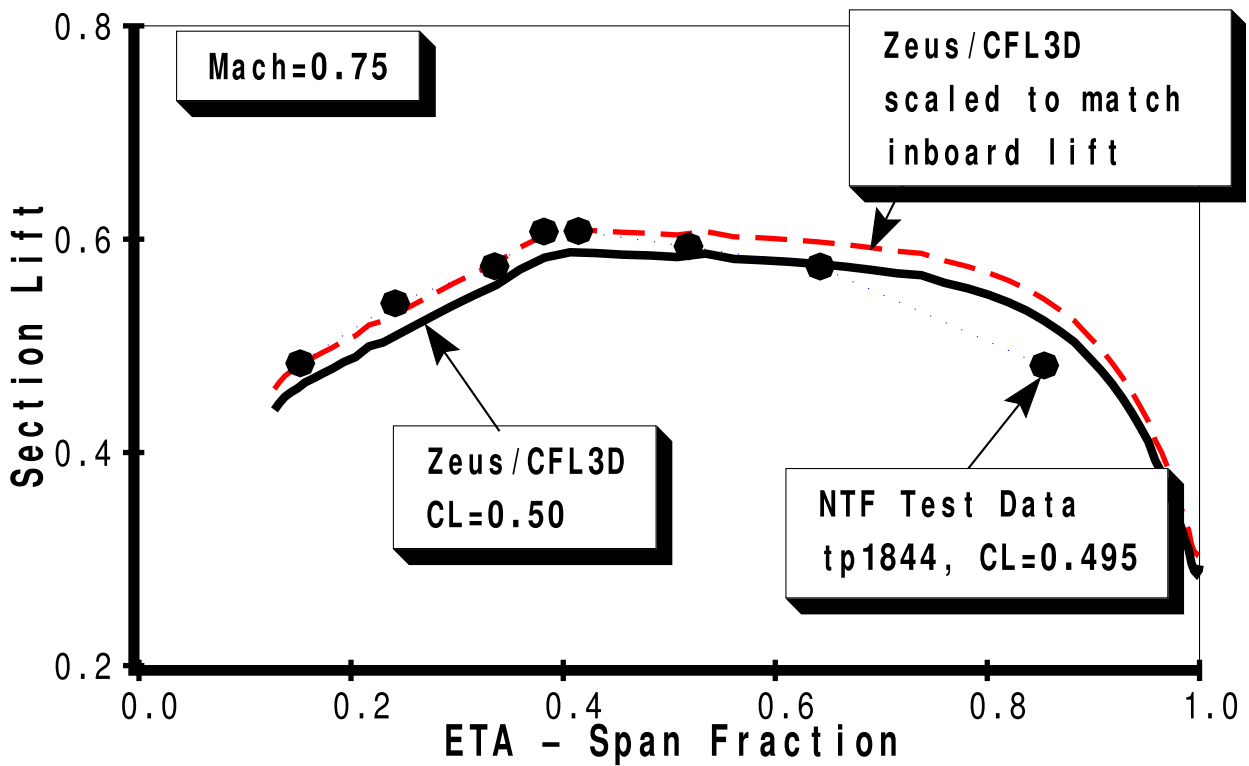

Figure 20. Spanload Comparison of NTF Data with CFL3D Results at the Design Point.